Hα3: an Hα imaging survey of HI selected galaxies from ALFALFA⋆

III. Nurture builds up the Hubble sequence in the Great Wall

G. Gavazzi[1], G. Savorgnan[1,2], M. Fossati[3,1], M. Dotti[1], M. Fumagalli[4,5]⋆⋆, A. Boselli[6], L. Gutiérrez[7], H. Hernández Toledo[8], R. Giovanelli[9], and M.P. Haynes[9]

[1] Università degli Studi di Milano-Bicocca, Piazza della Scienza 3, 20126 Milano, Italy
   e-mail: giuseppe.gavazzi@mib.infn.it
[2] Centre for Astrophysics and Supercomputing, Swinburne University of Technology, Hawthorn, Victoria 3122, Australia
   e-mail: gsavorgn@astro.swin.edu.au
[3] Max-Planck-Institut für Extraterrestrische Physik, Giessenbachstrasse, D-85748 Garching, Germany
   e-mail: mfossati@mpe.mpg.de
[4] Carnegie Observatories, 813 Santa Barbara Street, Pasadena, CA 91101, USA
   e-mail: mfumagalli@obs.carnegiescience.edu
[5] Department of Astrophysics, Princeton University, Princeton, NJ 08544-1001, USA
[6] Aix Marseille Université, CNRS, LAM (Laboratoire d'Astrophysique de Marseille) UMR 7326, 13388, Marseille, France
   e-mail: alessandro.boselli@oamp.fr
[7] Instituto de Astronomía, Universidad Nacional Autónoma de México, Carretera Tijuana-Ensenada, km 103, 22860 Ensenada, B.C., México.
   e-mail: leonel@astro.unam.mx
[8] Instituto de Astronomía, Universidad Nacional Autónoma de México, Apartado Postal 70-264, 04510 México D.F., México.
   e-mail: hector@astroscu.unam.mx
[9] Center for Radiophysics and Space Research, Space Science Building, Ithaca, NY, 14853
   e-mail: haynes@astro.cornell.edu, riccardo@astro.cornell.edu

ABSTRACT

Context. We present the analysis of Hα3, an Hα narrow-band imaging follow-up survey of galaxies selected from the HI Arecibo Legacy Fast ALFA Survey (ALFALFA) in the Coma supercluster.

Aims. Taking advantage of Hα3, which provides the complete census of the recent star formation in HI-rich galaxies in the local universe, we explored the hypothesis that a morphological sequence of galaxies of progressively earlier type and lower gas-content exists in the neighborhood of a rich cluster of galaxies such as Coma, with a specific star formation activity that decreases with increasing local galaxy density and velocity dispersion.

Methods. By using the Hα hydrogen recombination line as a tracer of the "instantaneous" star formation, complemented with optical colors from SDSS, we investigated the relationships between atomic neutral gas and newly formed stars in different local galaxy density intervals, for many morphological types, and over a wide range of stellar masses (10^9 to $10^{11.5}$ $M_\odot$).

Results. In the dwarf regime ($8.5 < \log(M_*/M_\odot) < 9.5$) we identify a four-step sequence of galaxies with progressively redder colors (corrected for dust extinction), i.e., of decreasing specific star formation, from (1) HI-rich late-type galaxies (LTGs) belonging to the blue cloud that exhibit extended plus nuclear star formation, (2) ∼ 0.1 mag redder, HI-poor LTGs with nuclear star formation only, (3) ∼ 0.35 mag redder, HI-poor galaxies without either extended or nuclear star formation, but with nuclear post-star-burst (PSB) signature, (4) ∼ 0.5 mag redder early-type galaxies (ETGs) that belong to the red sequence, and show no gas or star formation on all scales. Along this sequence the quenching of the star formation proceeds radially outside-in. The progression toward redder colors found along this "morphological" (gas content) sequence is comparable to the one obtained from increasing the local galaxy density, from cosmic filaments (1 2), to the rich clusters (2 3 4).

Conclusions. In the dwarf regime we find evidence for an evolution of HI-rich LTGs into ETGs through HI-poor LTGs and PSB galaxies driven by the environment. We identify ram-pressure as the mechanism most likely responsible for this transformation. We conclude that infall of galaxies has proceeded for the last 7.5 Gyr, building up the Coma cluster at a rate of approximately 100 galaxies with $\log(M_*/M_\odot) > 9.0$ per Gyr.

Key words. Galaxies: clusters: individual: Coma – Galaxies: fundamental parameters *luminosities, masses* – Galaxies: ISM

1. Introduction

Since the advent of the Sloan Digital Sky Survey (SDSS, York et al. 2000), which revolutionized research in astronomy at the turn of the millennium, surveys carried out at frequencies other than optical were designed with an extent, depth, and photomet-

ric and astrometric qualities comparable with SDSS.

One such ambitious survey is ALFALFA (Giovanelli et al. 2005), a blind HI sky survey that just ended at Arecibo (October 2012), aimed at obtaining the census of HI sources within 7000 sq degrees of the sky accessible from Arecibo, with an rms noise near 2 mJy after Hanning smoothing to 10 km s^{-1} (see Haynes et al. 2011), corresponding to $10^{7.7}$ M$_\odot$ of HI at the distance of Virgo and 10^9 M$_\odot$ at the distance of Coma. A catalog listing 40% of the whole ALFALFA sources available so far (α.40 catalog) has been published by Haynes et al. (2011).

The less extensive Hα3 is an Hα narrow-band imaging survey, ongoing at the 2.1m telescope of the San Pedro Martir (SPM) Observatory, aimed at following-up all nearby galaxies that are selected from ALFALFA in the redshift range ($-1000 < cz < 3000$ km s^{-1}) of the Local (Gavazzi et al. 2012) and Coma superclusters ($3900 < cz < 9500$ km s^{-1}). The sensitivity of Hα3 is such that galaxies with star formation rate (SFR) in excess of ~ 0.1 M$_\odot$ yr^{-1} are sampled up to the distance of Coma (100 Mpc). The three mentioned surveys provide us with the necessary ingredients for studying one of the most obvious, yet still unsettled questions of galaxy evolution: the transformation of primeval atomic gas (HI) into H$_2$, its fragmentation in molecular clouds, and the birth of new stars that contribute to the formation and evolution of galaxies. So far, the census of the SFR in the local Universe traced by hydrogen recombination lines has been determined on HI selected surveys, such as SINGG selected from HIPASS (Meurer et al. 2006), or optically selected ones (Boselli et al. 2001, Gavazzi et al. 2002b, 2006, James et al. 2004, Kennicutt et al. 2008, Lee et al. 2007, 2009, Bothwell et al. 2009), or in optically selected galaxies with stellar mass larger than 10^{10} M$_\odot$ (e.g. GASS, the GALEX Arecibo SDSS Survey, Catinella et al. 2010, Schiminovich et al. 2010, Fabello et al. 2012). The combined sensitivities of SDSS, ALFALFA, and Hα3 are such that the present analysis can be extended to dwarf galaxies with stellar masses as small as 10^8 M$_\odot$. Combining the α.40 catalog (Haynes et al. 2011) with the catalog provided by the legacy program carried out with the Galaxy Evolution Explorer (GALEX), Huang et al. (2012) carried out the most recent investigation of the scaling relations between HI gas, star formation[1], and stellar mass. They did not touch on the debated question whether the transformation of gas into stars which has provided the build-up of the Hubble sequence over the cosmic time, depends on the environment (nurture) or is a purely "genetic" process (nature), which is the focus of the present work. We follow the line traced by Boselli et al. (2008) and by Paper II (Gavazzi et al. 2013a), who found evidence that a strong role is played by the environment in the Virgo cluster for the transformation of star-forming dwarf galaxies of late type into quiescent dwarf elliptical galaxies due to the fast ablation of the interstellar gas caused by the ram-pressure mechanism (Gunn & Gott 1972), with consequent suppression of the star formation. Moreover, we continue on this line, following Gavazzi et al. (2010), who found support for these ideas by studying the population of late-type galaxies surrounding the Coma cluster using photometry and spectroscopy from the SDSS to separate the stellar populations in galaxies as faint as M_i=-17.5 mag. The Coma supercluster consists of a main filament of galaxies running perpendicularly to the line of sight across several hundreds of Mpc, with a

distribution of galaxies spanning a significant density contrast. Its very shape, along with the new available data on the HI gas content from ALFALFA and the measurements of the star formation provided by Hα3, offer a unique opportunity of pursuing this question in the present Paper III of the Hα3 series.

Paper III is structured as follows. The optical- and radio-selected samples used in the analysis are defined and discussed in Section 2. Section 3 contains the evidence of the environmental dependency of the gas content and of the star formation activity (both in the disk and circumnuclear). Discussion and summary are given in Section 4. A method for correcting the optical colors for internal extinction is obtained in Appendix A. The scaling relations between HI mass, stellar mass and the star formation in Coma compared to the Local Supercluster are discussed in Appendix B.

The Hα3 observations of the Local Supercluster have been the subject of Paper I of this series (Gavazzi et al. 2012). Paper II (Gavazzi et al. 2013a) outlined the analysis, including the study of the scaling relations between HI mass, stellar mass, star formation, and the environmental conditions. Paper IV (Fossati et al. 2013) will analyze the structural properties of galaxies in the Local and Coma superclusters, and Paper V (Gavazzi et al. 2013b) will contain the Hα3 data (fluxes and images) in the Coma supercluster.

2. The Sample

The present analysis is focused on galaxies members of the Coma supercluster, which belongs to three subsamples: sample 1 is composed of 5026 optically selected galaxies brighter than $r \leq 17.77$ (and is complete to this limit), sample 2 consists of 683 HI-selected galaxies (from ALFALFA), sample 3 (a subset of sample 2) consists of 383 galaxies that were followed-up with Hα observations as part of Hα3.

The sky distribution of the Great Wall is displayed in the top panel of Figure 1, while a wedge diagram of the HI-selected sample is shown in the bottom panel. The optically selected sample was built from the union of two regions: region 1 with $172^\circ < $ R.A. $ < 202^\circ$; $18^\circ < $ Dec. $ < 32^\circ$ ($11.5^\mathrm{h} < $ R.A. $ < 13.5^\mathrm{h}$, gray shaded in Figure 1), which traditionally describes the Coma supercluster, and region 2 with $150^\circ < $ R.A. $ < 240^\circ$; $24^\circ < $ Dec. $ < 28^\circ$ ($10^\mathrm{h} < $ R.A. $ < 16^\mathrm{h}$, blue-shaded in Figure 1) covered by ALFALFA. In both regions we limit our analysis to the redshift interval $3900 < cz < 9500$ km s^{-1}, chosen to comprise the "finger of God" of the Coma cluster.

2.1. Optically selected sample

Galaxies belonging to the Coma supercluster, which lies at a mean distance of 100 Mpc, have apparent radii small enough that their SDSS images are only little affected by the "shredding" of large galaxies into multiple pieces, which leads to wrong magnitude determinations[2] (Blanton et al. 2005a,b,c). Hence a reliable optically selected sample can be extracted from the SDSS spectroscopic database following the criteria described in Gavazzi et al. (2010, 2011) which we only briefly summarize here. We searched the SDSS DR7 spectroscopic database (Abazajian et al. 2009) in regions 1 and 2 (see Figure 1) for all galaxies with

---

[1] We emphasize that the SFR in normal galaxies can be estimated from the UV provided that this remained constant over a time scale $t < 10^8$ yr. In contrast if the SFR changed during a time scale $10^7 < t < 10^8$ yr, which is most likely the case of cluster and dwarf galaxies, the most appropriate SFR indicator is Hα (Boselli et al. 2009).

[2] Shredding of large galaxies is caused by the combined effect of cutting the images of individual galaxies into multiple pieces, due to the observing strategy of SDSS by discrete "tiles", and to the inefficiency of Sextractor (Bertin & Arnouts 1996) in reconstructing the total flux of very extended objects.
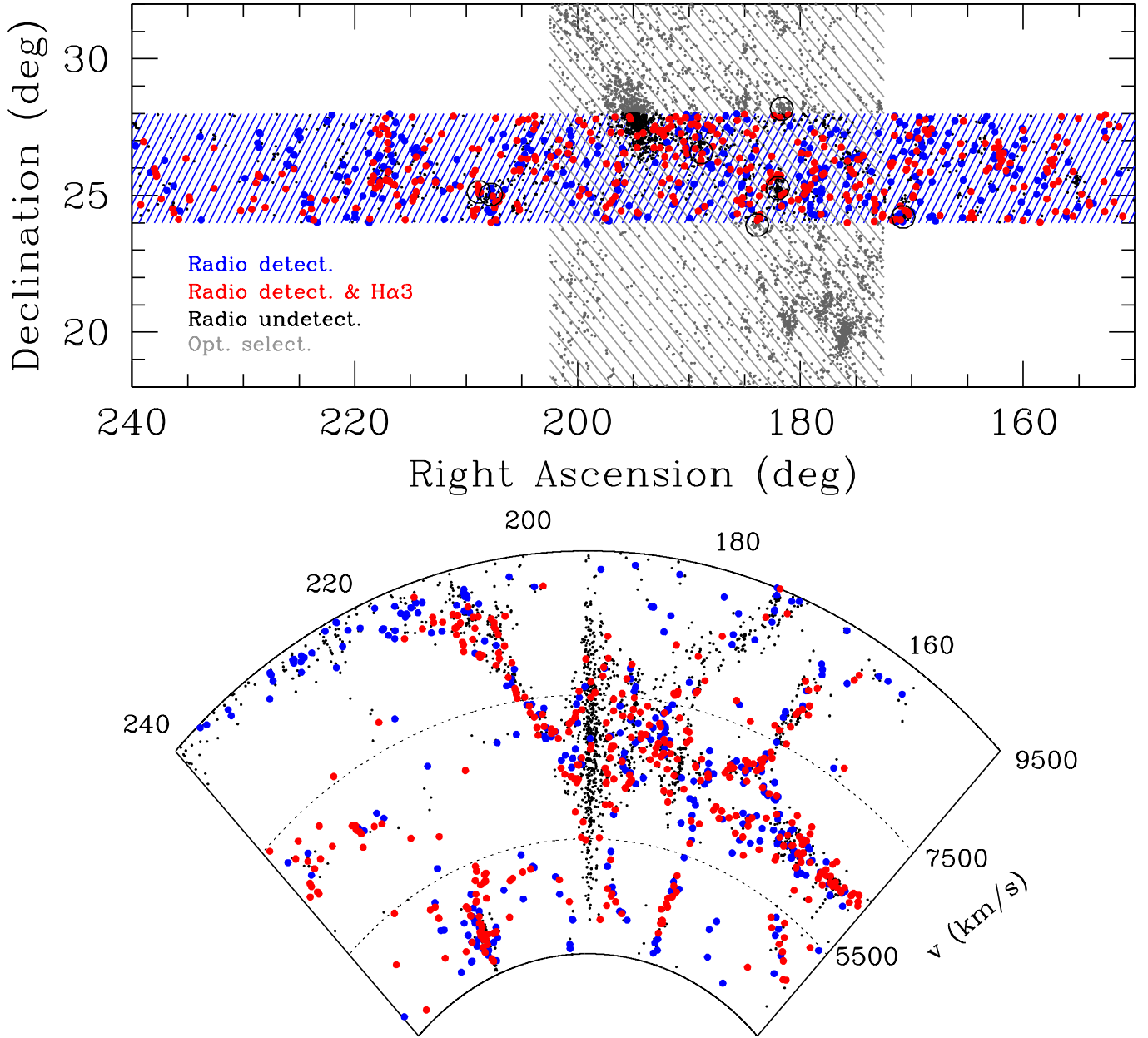
Fig. 1. Top panel: sky distribution (the R.A. scale is compressed) of the Coma supercluster area studied in this work, constituted by the union of the traditional area occupied by the Coma supercluster $172° < $ R.A. $< 202^o$; $18^o < Dec. < 32^o$ (region 1, gray shaded) with the elongated region $150° < $ R.A. $< 240^o$; $24° < $ Dec. $< 28^o$ (region 2, blue shaded) covered by ALFALFA (Haynes et al. 2011). In both regions only galaxies in the interval $3900 < cz < 9500$ km s^{-1} are considered. Sample 1 includes 5026 galaxies of all morphological types optically selected from SDSS (small black dots) in the union of regions 1+2. Sample 2 includes 683 galaxies HI selected from ALFALFA (blue symbols). Sample 3 (a subset of sample 2) is composed of 383 galaxies followed-up with Hα observations as part of Hα3 (red symbols). Region 1 will be fully covered by ALFALFA in the near future. Currently, only the brightest galaxies have been observed in HI and in Hα with pointed observations (listed in GOLDmine). Black circles mark the position of the seven groups found in region 2. Bottom panel: recessional velocity versus R.A. distribution of 2416 galaxies in the region 2 covered by ALFALFA (black). 683 galaxies detected by ALFALFA are represented in blue. The 383 galaxies observed in Hα as part of Hα3 are plotted in red. Note the filamentary structure departing from the Coma cluster (identified by the "finger of God" near R.A.=195), with increasing velocity toward the Hercules supercluster (R.A.= 240).

$r \leq 17.77$ mag, which matches the selection criterion of the SDSS spectral catalog (Strauss et al. 2002), in the redshift interval $3900 < cz < 9500$ km s^{-1}. We obtained 4790 targets. For each, we extracted the coordinates, the u, g, r, i, z Petrosian magnitudes (AB system, not corrected for internal extinction), and the spectroscopic information, including the principal (nuclear) line intensities and the redshift. The morphological classification of all galaxies was performed by individual visual inspection of SDSS color images.

To fill in the incompleteness of SDSS for luminous galaxies due to shredding and fiber conflict, we added 133 CGCG (Zwicky et al. 1961-1968) galaxies with known redshifts from NED that were not included in the SDSS spectral database. For these objects, we also took the u, g, r, i, z Petrosian magnitudes using the SDSS DR7 navigation tool, which provides accurate magnitudes. Additional galaxies that could not be found in the SDSS spectroscopic catalog were searched for using NED. For these targets, we again evaluated the u, g, r, i, z magnitudes using the SDSS navigator, and of these we selected 76 objects that meet the condition $r \leq 17.77$ mag. We repeated a similar search in the ALFALFA database (Haynes et al. 2011) in region 2, where we found 28 additional HI-selected systems with $r \leq 17.77$ mag, that were not included in the SDSS spectral database.

In total, our optical sample consists of 5026 galaxies: 4790 from SDSS and 236 from other sources. Of the 5026, 2146 galaxies lie in region 2.

The stellar mass was derived from the i magnitudes and $g - i$ color using the transformation

$$\log\left(\frac{M_*}{M_\odot}\right) = -1.94 + 0.59 \cdot (g - i) + 1.15 \cdot \log\left(\frac{L_i}{L_\odot}\right), \quad (1)$$

where $\log L_i$ is the i band luminosity in solar units ($\log L_i = (I - 4.56)/ - 2.5$). This is a modification of the Bell et al. (2003) formula that we computed to be consistent with the mass determination of Brinchmann MPA-JHU[3].

Following a procedure identical to the one used in Gavazzi et al. (2010, 2011), the local number density ρ around each galaxy was computed within a cylinder of $1~h^{-1}$ Mpc radius and 1000 km s^{-1} half-length. Around each galaxy we computed the 3-D density contrast as

$$\delta_{1,1000} = \frac{\rho - <\rho>}{<\rho>}$$

, where ρ is the local number density and $<\rho> = 0.05$ gal $(h^{-1}$ Mpc$)^{-3}$ represents the mean number density measured in the whole region. We divided the sample into four overdensity bins, chosen to highlight physically different environments of increasing level of aggregation: the ultra-low density bin (UL: $\log(1+\delta_{1,1000}) \leq 0$) that describes the underdense cosmic structures (sparse filaments and voids); the low-density bin (L: $0 < \log(1 + \delta_{1,1000}) \leq 0.7$) that comprises the filaments in the Great Wall and the loose groups; the high-density bin (H: $0.7 < \log(1 + \delta_{1,1000}) \leq 1.3$) that includes the cluster outskirts and the significant groups; and the ultra-high density bin (UH: $\log(1 + \delta_{1,1000}) > 1.3$) that corresponds to the cores of rich clusters.

2.2. HI-selected sample

The HI-selected sample analyzed in this work is drawn from the 360 square degree region 2. This region has been fully mapped by ALFALFA, providing us with a complete sample of HI-selected galaxies (Haynes et al. 2011). At present, half of the Coma cluster lies within the footprint of ALFALFA.

The completeness and sensitivity of ALFALFA are clearly described and discussed in detail in Saintonge (2007), Martin et al. (2010), and Haynes et al. (2011). An estimate of the limiting
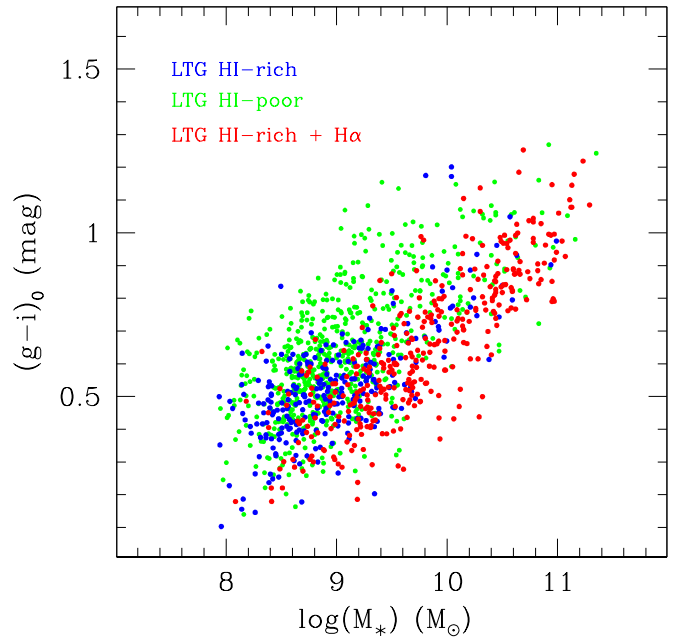
Fig. 2. Corrected color $(g - i)_o$ vs. stellar mass diagram of optically selected galaxies limited to LTGs (subsample 2). The colors are corrected for extinction in the Milky Way and for internal extinction according to the prescriptions of Appendix A. LTGs undetected by ALFALFA are represented by green symbols. LTGs detected by ALFALFA are given in blue. Red symbols denote the subsample of the ALFALFA-selected galaxies that were followed-up in Hα3.

sensitivity of ALFALFA at the distance of Coma can be obtained using equation 1 in Giovanelli et al. (2007):

$$S/N = \left(\frac{1000 \cdot S_{21}}{W_{50}}\right) \cdot \frac{w_{smo}^{1/2}}{\sigma_{rms}}, \quad (2)$$

where S_{21} is the integrated flux under the HI profile in units of Jy km s^{-1}, w_{smo} is a smoothing width expressed as the number of spectral resolution bins of 10 km s^{-1} that bridges half of the signal width. W_{50} is the profile width at 50% of the height and σ_{rms} is the typical noise in the baseline in bins of 10 km s^{-1}. For $W_{50} < 400$ km s^{-1}, $w_{smo} = W_{50}/(2 \cdot 10)$. The HI mass is $M_{HI} = 2.36 \cdot 10^5 \cdot S_{21} \cdot D^2$, where D is the distance to the source in Mpc.

The limiting HI mass of ALFALFA can be computed as

$$M_{HI,lim} = 2.36 \cdot 10^5 \cdot D^2 \cdot (W_{50} \cdot 20)^{1/2} \cdot \sigma_{rms} \cdot S/N_{lim}, \quad (3)$$

where $W_{50} = W_{50,0} \cdot \sin(incl)$ ($W_{50,0}$ is the face-on line width) and $incl$ is the galaxy inclination in the plane of sky determined from equation (A1).

Adopting $\sigma_{rms} = 2.1$ mJy, typical of ALFALFA spectra, the mean distance to Coma $D = 100$ Mpc, $S/N_{lim} = 6.5$ and $W_{50,0} = 100$ km s^{-1}, we obtain $\log(M_{HI,lim}/M_\odot) = 8.78, 9.08, 9.15$ for $incl$=10, 45, 70 deg[4]. In conclusion, ALFALFA is sensitive to galaxies that contain approximately $\log(M_{HI}/M_\odot) \sim 9$ at the distance of Coma.

2.3. Hα sample

Hα3 consists of follow-up Hα observations of 383 galaxies among the HI-selected (detected) ones. These data, resulting from the joined effort by the Hα3 collaboration in 2010, 2011 and 2012 using the 1.5m and 2.1m telescopes at SPM, will be discussed in full detail (and publicly released) in Paper V of this series. Starting from 683 ALFALFA targets with high signal-to-noise (typically S/N > 6.5) and a good match between two independent polarizations (code = 1 sources; Giovanelli et al. 2005, Haynes et al. 2011), in the first two years (2010, 2011) our observational effort had been focused on radio targets brighter than 1 Jy km s^{-1} and with $3900 < cz < 9000$ km s^{-1}, while fainter targets were observed in 2012. However, approximately 95 additional bright CGCG galaxies (Zwicky et al. 1961-1968) in the intersection between region 1 and 2 (11.5^h < R.A. < 13.5^h; 24° < Dec. < 28°) and 207 additional CGCG galaxies outside region 2 were already observed in Hα by Gavazzi et al. (1998, 2002a, 2002b, 2006), Boselli & Gavazzi (2002), and Iglesias Paramo et al. (2002). For these targets images and fluxes are publicly available via the GOLDmine web server (Gavazzi et al. 2003). In total, the number of galaxies in Sample 3 (Hα3) is 383, but the total number of galaxies observed in Hα is 95+383+207=685. For these targets the SFR was computed from the luminosity of the Hα line after correcting for Galactic extinction and after the Hα line was deblended from the contribution from [NII] emission using the criteria adopted in Paper I. Based on the mass-metallicity relation (Tremonti et al. 2004), we calibrated a relation between the ratio N[II]/Hα and the absolute i band magnitude, excluding active galactic nuclei (AGNs). Details on these quantities will be given in Paper V. No correction for internal dust extinction has been applied because very few drift-scan spectra are available from Gavazzi et al. (2004) and Boselli et al. (2013), which are necessary to estimate the Balmer decrement and in turn the extinction coefficient A(Hα) on the full disk scale. The SDSS spectra could not provide for this correction because, at the distance of Coma, they cover just the nuclear galaxy region and hence are not representative of the whole galaxy.

Summarizing, ALFALFA provides us with the HI mass of LTGs complete to approximately 10^9 M$_\odot$, whose optical colors (corrected for internal extinction according to the prescriptions of Appendix A) and stellar masses are distributed as shown in Figure 2. The figure highlights that only the part of the "blue cloud" composed of HI-rich LTGs is sampled by ALFALFA (blue + red symbols), whereas LTGs that have less than 10^9 M$_\odot$ of HI, hereafter considered HI-poor LTGs, are not detected by ALFALFA (green symbols). We highlight the subsample of ALFALFA targets that were followed-up in Hα3 with red symbols.

3. Environmental Effects

3.1. Pattern of HI-deficiency

It has long been known that the HI-deficiency parameter (Def_{HI}) is perhaps the most reliable indicator of whether or not an LTG belongs to the harsh environment of a rich cluster (Giovanelli & Haynes, 1985). Def_{HI} has been defined by Haynes & Giovanelli (1984) as the logarithmic difference between the HI mass observed in an object and the expected value in isolated and unperturbed objects of similar morphological type T and linear diameter D_{25}: $Def_{HI} = \langle \log M_{HI}(T, D_{25}) \rangle - \log M_{HI}^{obs}$. Here, $\langle \log M_{HI}(T, D_{25}) \rangle = C_1 + C_2 \times 2 \log D_{25}$, where D_{25} (in kpc) is determined in the g band at the 25th mag arcsec^{-2} isophote. The coefficients C_1 and C_2 were determined by Haynes & Giovanelli
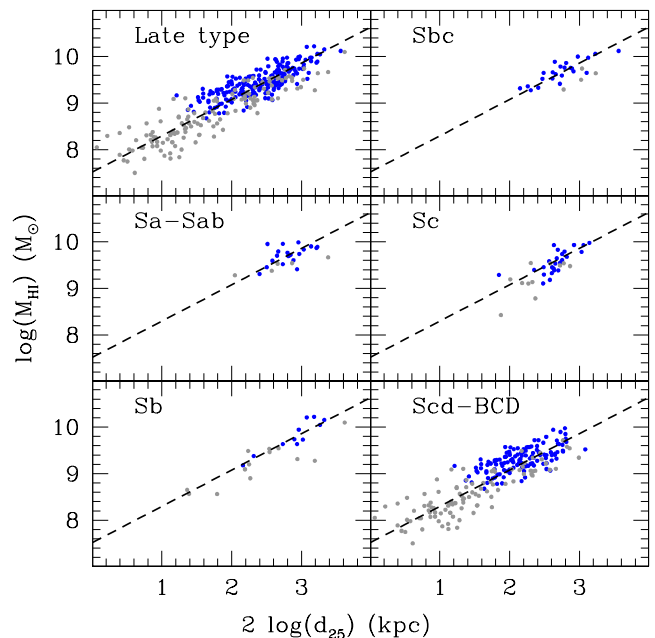

Fig. 3. $\log M_{HI}(T, D_{25})$ relation for isolated galaxies with $\delta_{1,1000} < 0$ in the Coma supercluster (blue) and in the Local Supercluster (Paper II; gray). The fit obtained using all late-type (Sa-BCD) objects is given as a dashed line in every panel.
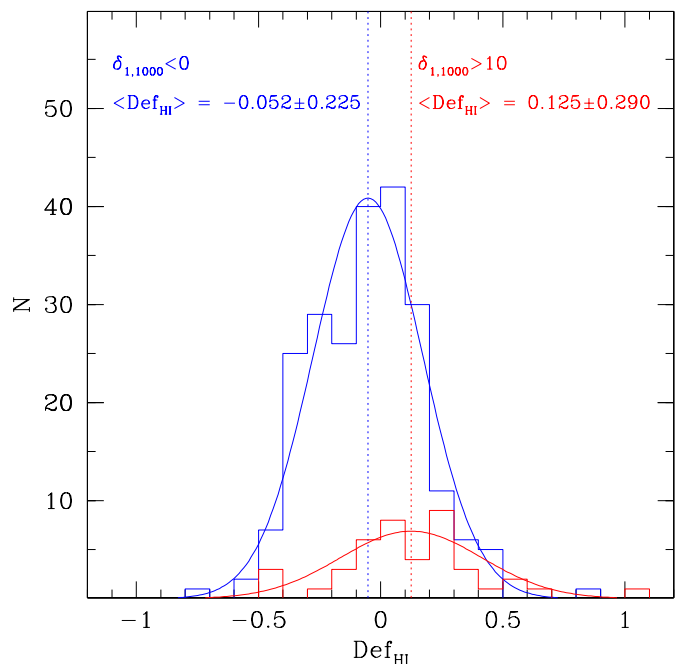

Fig. 4. Histogram of the Def_{HI} parameter derived from ALFALFA observations of the Coma supercluster, separately for isolated objects with $\delta_{1,1000} < 0$ (blue) and for galaxies in the densest regimes ($\delta_{1,1000} > 10$ red).

(1984) by studying a control sample of isolated objects, and later, on a larger sample by Solanes et al. (1996). Both samples are composed almost exclusively of giant spirals however. The HI deficiency parameter was therefore poorly calibrated for dwarf objects. This problem was addressed in Paper II, where
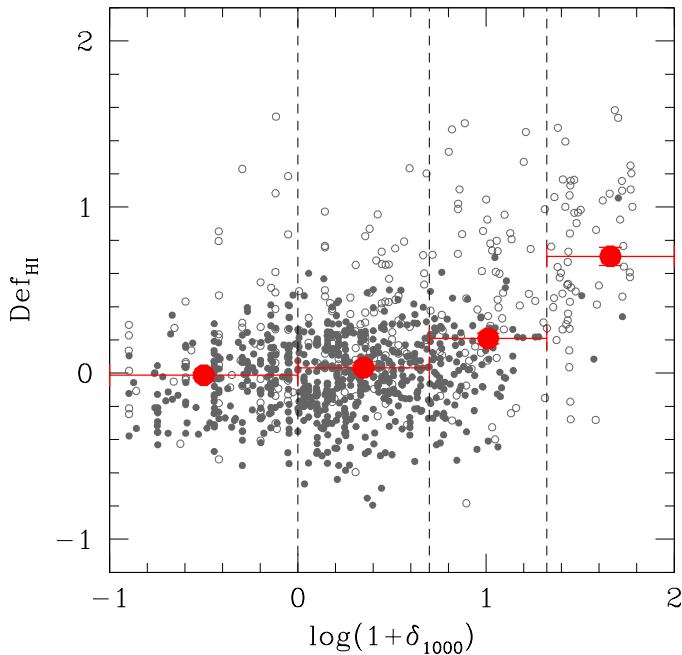
Fig. 5. Distribution of the Def_{HI} parameter of galaxies in the Coma supercluster as a function of the local galaxy density $\delta_{1,1000}$. Filled dots represent HI data from ALFALFA, empty symbols derive from deeper, pointed HI measurements of optically selected galaxies. Clearly ALFALFA is not sufficiently deep to detect deficient objects, except for few massive, face-on galaxies (the only point above Def_{HI}=1 is NGC 4921, a face-on giant Sb in the Coma cluster). Deeper, pointed HI observations reveal the expected increase of the mean HI deficiency with increasing local galaxy density (red symbols).

Fig. 6. The fraction of LTGs (in region 2) detected by ALFALFA (blue histogram); undetected by ALFALFA (green histogram); PSB (black histogram), in four bins of increasing local density (representing the sparse cosmic web, the filaments, the groups and the cluster's cores).

the relatively isolated galaxies in the Local Supercluster were used to determine that C_1=7.51 and C_2=0.68 hold for all LTGs. Here, combining isolated LTGs from the Local Supercluster with the lowest density objects in the Coma supercluster we obtain C_1=7.50 and C_2=0.79, consistently with the Local Supercluster alone (and with the Coma1 cloud, see Boselli & Gavazzi 2009). These coefficients are consistent with those adopted by Solanes et al (1996) up to Sc galaxies, and by Toribio et al. (2011) up to Scd-Sd galaxies.

Figure 3 shows the relations among M_{HI} and the diameters found adopting these coefficients. The fit[5] obtained for all LTGs is depicted with the dashed line. The distribution of the Def_{HI} parameter of galaxies in the Coma supercluster is plotted in Figure 4 separately for $\delta_{1,1000} < 0$ (isolated objects, blue) and $\delta_{1,1000} > 10$ (rich clusters, red), with the mean Def_{HI} obtained in the two bins (intermediate-density objects are not plotted, but are considered in the following analysis). Apparently, isolated objects have a mean deficiency consistent with 0 ± 0.2. Throughout this paper we consider as "normal" or "unperturbed" by the cluster environment, as far as their HI content is concerned, 270 galaxies with $Def_{HI} \leq 0.2$, i.e., within $1~\sigma$ of the mean deficiency of the isolated sample. At the distance of Coma, galaxies with $Def_{HI} > 0.2$ are undersampled because they lie below the sensitivity of ALFALFA.

Figure 5 shows the deficiency parameter plotted as a function of the local density. Filled symbols refer to galaxies in the HI-selected sample, i.e., detected by ALFALFA. Evidently, as the galaxy density $\log(1+\delta_{1,1000})$ approaches 1 (the cluster outskirts) ALFALFA detects almost no galaxies, because they are too shallow to reveal the Giovanelli & Haynes (1985) pattern of HI deficiency near the Coma cluster. However, when pointed long-integration HI observations deeper than ALFALFA are considered, such as those available for region 1 from GOLDmine (open gray symbols with red binned averages), the expected increase of Def_{HI} with local density clearly appears.

3.2. What do the LTGs undetected by ALFALFA represent?

In contrast to the Local Supercluster (Paper II of this series), the sensitivity of ALFALFA at Coma is insufficient for detecting galaxies with significant HI deficiency (see previous section)[6]. The known trend of increasing HI deficiency with increasing galaxy density (see Figure 4) could be revealed only using the long-integration pointed radio detections available in region 1. Therefore a discussion similar to Paper II, where some galaxy properties were analyzed in bins of increasing Def_{HI}, cannot be undertaken. Moreover, because Hα3 suffers from the same selection bias as ALFALFA, no trends between the SFR and the HI deficiency can be directly investigated.

This problem can be addressed, however, by separating LTGs that were detected/undetected by ALFALFA. As already stressed in Paper I, the radio selection biases Hα3 toward HI-rich LTGs (see also Gavazzi et al. 2008). ALFALFA detects almost exclusively LTGs in the blue sequence, not all LTGs are detected (see green symbols in Figure 2). As we showed in Paper II and in Gavazzi et al. (2008), where we focused on galaxies in the Local

---

[5] Linear regressions are obtained in this work using the bisector method (mean coefficients of the direct and the inverse relation, Isobe et al. 1990).
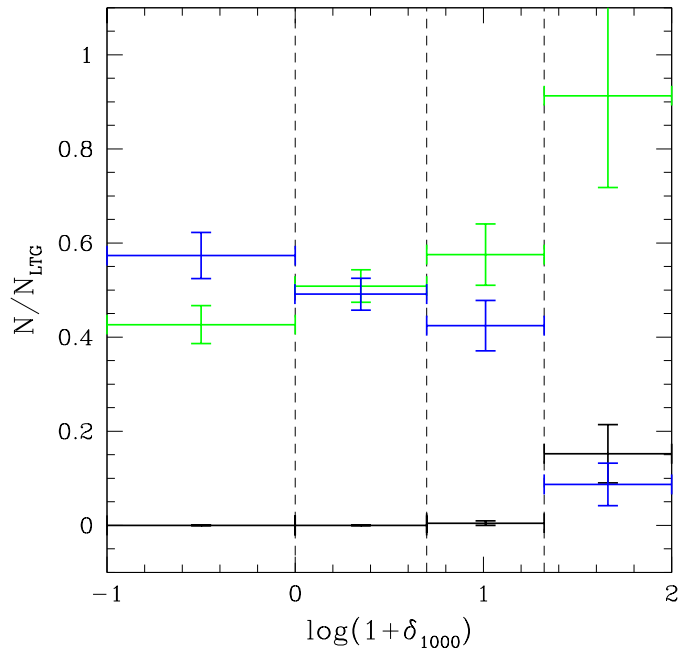
[6] We recall that ALFALFA is a two-passes survey of approximately 7000 sq degrees visible from Arecibo. To make it sensitive to 10^8 M$_\odot$ of HI at the distance of Coma, it would require some 500,000 hours of telescope time!

Supercluster, the very existence of a limiting HI mass combined with the relation $\log M_{\mathrm{HI}} = 0.52 \times \log M_* + 4.54$ (see Appendix B) that holds for normal galaxies induces an optical limit for the detection of HI-rich systems. At the distance of Coma, galaxies fainter than $\log(M_*/\mathrm{M}_\odot) \sim 8.5$ or $M_i \sim -17$ mag are not detected by ALFALFA. Furthermore, even some late-type galaxies brighter than this limit are not detected in ALFALFA or in Hα3. LTGs that are not detected by ALFALFA are truly HI-poor systems[7].

Figure 6 sheds more light on the nature of HI-poor LTGs by plotting their frequency distribution as a function of the local galaxy density: the fraction of HI-rich LTGs detected by ALFALFA (blue histogram), representing about 50% of all LTGs in the field, decreases gradually with increasing density and drops to zero in the core of Coma; the fraction of HI-poor LTGs undetected by ALFALFA (green histogram), representing the remaining 50% of all LTGs in the field, increases with increasing density to nearly 100%. Incidentally, the fraction of post-star burst systems is null in the field, in filaments, and in groups but it becomes significant in the core of Coma (see also Gavazzi et al. 2010). Summarizing, when galaxies approach denser environments, their gas content is progressively reduced, which mimics the pattern of morphology segregation.

3.3. Color, HI content, and local density

We now show that HI-poor LTGs are statistically less star-forming than their HI-rich counterparts of similar stellar mass. Figure 7a shows the color-mass relation of galaxies, divided into four groups of different morphological type/gas-content: HI-rich (detected by ALFALFA) LTGs are plotted with blue symbols; HI-poor (undetected by ALFALFA) LTGs are marked with green symbols, PSB galaxies identified by Gavazzi et al. (2010) are shown with large black symbols[8], and red symbols represent early-type galaxies that belong to the red sequence.

Late-type galaxies that are not detected by ALFALFA (green symbols), dubbed HI-poor LTGs, lie nearer to the "green valley" than ALFALFA detected galaxies (blue symbols) even though they belong to the sequence of LTGs. For all types of galaxies, Figure 7a reports the linear fit of the color-stellar mass relation. The four galaxy groups, selected by their optical morphology/gas content and nuclear spectral properties, have increasingly redder colors, i.e., decreasing SSFR. Despite the paucity of Hα measurements (particularly of HI-poor and ETGs), Figure 7c supports the idea that the color-mass sequence is indeed a star formation-mass sequence. Here we plot the specific star formation rate (SSFR), i.e., the star formation rate per unit stellar mass, as derived from our Hα data for ALFALFA-detected (blue sym-

bols) and for the few HI-poor (green symbols) and ETGs (red symbols) that are included in Hα3, with their linear fits[9].

There is a qualitative correspondence (albeit with a large scatter) between the classification given in Fig 7a, based on morphology, and the one given in in Figure 7b, based on local galaxy density: HI-rich LTGs detected by ALFALFA have mean $\delta_{1,1000} = 1.7 \pm 4.3$, typical of the sparse galaxy population; HI-poor LTGs undetected by ALFALFA have mean $\delta_{1,1000} = 4.8 \pm 11$, typical of the outskirts of rich clusters and of the densest groups; galaxies with nuclear post-star-burst spectra (PSB) and passive ETGs have mean $\delta_{1,1000} = 23 \pm 20$, implying that they are found primarily in the cores of rich clusters.

A quantitative assessment of the median $(g - i)_o$ color in different classes of morphology/HI content and its correspondence with the median $(g - i)_o$ color in different classes of local galaxy density is given in Figure 8, referring only to the low-mass interval $8.5 < \log(M_*/\mathrm{M}_\odot) < 9.5$. The left panel shows the cumulative $(g - i)_o$ distribution of galaxies (in region 2), selected according to a criterion of decreasing "lateness"[10]:

- HI-rich LTGs ($8.5 < \log(M_*/\mathrm{M}_\odot) < 9.5$) (blue)
- HI-poor LTGs ($8.5 < \log(M_*/\mathrm{M}_\odot) < 9.5$) (green)
- PSB galaxies ($8.5 < \log(M_*/\mathrm{M}_\odot) < 9.5$) (black)
- ETG galaxies ($8.5 < \log(M_*/\mathrm{M}_\odot) < 9.5$) (red),

The median $(g - i)_o$ color increases step by step from 0.50, 0.59, 0.84, to 1.00 mag along this sequence, which thus represents a sequence of decreasing specific star formation. The right panel shows the cumulative $(g - i)_o$ distribution of galaxies of any morphological type, selected in bins of increasing (not necessarily contiguous) local galaxy density: from $\log(1 + \delta_{1,1000}) < -0.5$ (blue), $0 < \log(1 + \delta_{1,1000}) < 0.4$ (green), $0.5 < \log(1 + \delta_{1,1000}) < 1.35$ (cyan), $1 < \log(1 + \delta_{1,1000}) < 1.5$ (black) to $\log(1 + \delta_{1,1000}) > 1.5$ (red). In this case the median $(g - i)_o$ color increases step by step from 0.53, 0.57, 0.75, 0.94, to 1.00 mag, which agrees well with the previous series, so the shape of the distributions is remarkably similar, despite the completely independent criteria in choosing the morphological intervals and the density intervals. It should be remarked that this result holds for galaxies in the low-mass interval $8.5 < \log(M_*/\mathrm{M}_\odot) < 9.5$ only. We have checked that for $\log(M_*/\mathrm{M}_\odot) > 9.5$ the data do not support a similar pattern with increasing ambient galaxy density. Consistently with Gavazzi et al. (2010) we conclude that nurture works in the low mass regime, while other genetic processes, namely *downsizing*, have shaped the high-mass part of the red sequence earlier in the cosmic history. In the high-mass regime Mendel et al. (2012) have suggested that the quenching of the star formation, leading to the transition from star-forming to passive galaxies, is driven by the formation of stellar bulges.

Figure 9 is useful for discussing the dependence of the $(g-i)_o$ color on the local galaxy density, separately for galaxies less and more massive than $\log(M_*/\mathrm{M}_\odot) = 9.5$. First, the massive galaxies have a well-developed red sequence even at galactic densities

---

[7] Before assuming that all galaxies undetected by ALFALFA are intrinsically HI-poor, i.e., have $\log(M_{\mathrm{HI}}/\mathrm{M}_\odot) < 9$, one must exclude the optical targets undetected by ALFALFA due to confusion in the Arecibo beam by other detected galaxies at similar velocity. Using a 3.5 arcmin FWHM beam and $\Delta V = 200$ km s^{-1} at the position of each detected target, we found only 28 optically selected candidates that were confused (roughly 1% of all galaxies in region 2 and 4% of all undetected LTGs). We thus conclude that most undetected LTGs with $\log(M_*/\mathrm{M}_\odot) > 9$ are truly HI-poor systems. Indeed, using pointed observations available from Arecibo for LTGs in the intersection between region 1 and region 2, we determined that $< Def_{\mathrm{HI}} >= 0.13$ for LTGs detected by ALFALFA, while $< Def_{\mathrm{HI}} >= 0.73$ for LTGs undetected by ALFALFA.

[8] A confirmation that PSB galaxies are low-mass objects that fill the "green valley" between star-forming and passive galaxies was derived for the galaxy Zoo by Wong et al. (2012).

[9] By selection we have very few Hα images of HI-poor galaxies (either ETGs or LTGs) because, as they are not in the ALFALFA sample, they are excluded also from Hα3. However, a few dozen of them were serendipitously observed, some on purpose, during the 2012 run. In particular the 80 measurements for ETGs belong for the most part to S0 (19) and S0a (38). Their SFR is derived from the intensity of the Hα line.

[10] Along with these four categories, Figure 8 also reports with cyan symbols the intermediate interval that contains HI-poor galaxies of any morphological type for completeness. The median color in this interval is 0.81 mag.
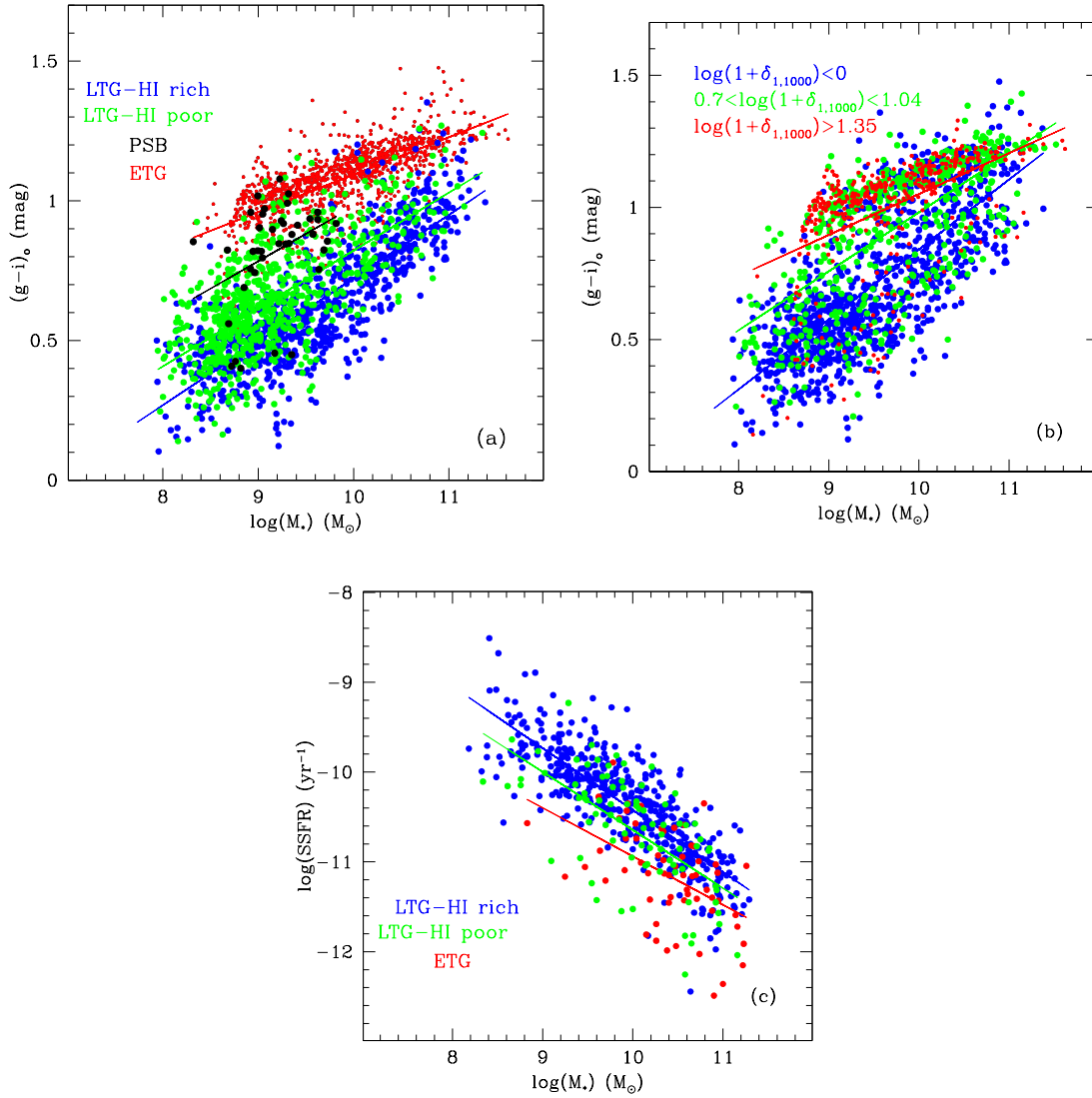
Fig. 7. Four-step sequence of galaxies of increasing $(g-i)_o$ color is identified in the color-mass diagram of panel (a) when four groups of different morphological types/gas-content/nuclear properties are considered. Panel (a): corrected color $(g-i)_o$ vs. stellar mass diagram of optically selected galaxies of all morphological types. Red symbols represent ETGs. Green symbols represent HI-poor LTGs not detected by ALFALFA, while HI-rich LTGs detected by ALFALFA are given in blue. Large black symbols represent PSB (also named k+a, i.e., with Balmer lines in absorption) galaxies identified by Gavazzi et al. (2010). They all lie at $\log(M_*/M_\odot) < 10$. Panel (b): a similar gradual trend in the color-mass diagram is found when galaxies are grouped in bins of increasing local density. This panel shows the corrected color $(g-i)_o$ vs. stellar mass diagram of optically selected galaxies of all morphological types, in three bins of decreasing local density: red= $\log(1 + \delta_{1,1000}) > 1.35$, green= $0.7 < \log(1+\delta_{1,1000}) < 1.04$; blue= $\log(1+\delta_{1,1000}) < 0$. Panel (c): the specific star formation rate (SSFR) vs. stellar mass diagram of galaxies covered by ALFALFA and followed-up by Hα3. Galaxies are color-coded according to the following criterion: red = ETGs; green = LTGs undetected by ALFALFA (HI-poor); blue = LTGs detected by ALFALFA (HI-rich). Unsurprisingly, the statistics are very poor among ETGs and for HI-poor LTGs.

as low as $\log(1 + \delta_{1,1000}) = -0.5$, while for the less massive objects the red sequence exists only above $\log(1 + \delta_{1,1000}) > 0.5$, in agreement with Gavazzi et al. (2010). Second, galaxies in the red sequence dominate in number the distribution of the massive galaxies, while the reverse is true for low-mass galaxies. Third, blue-sequence galaxies are more abundant at low density, where the red sequence is coarser and the number of PSB galaxies is relevant only at low mass, in agreement with Gavazzi et al. (2010) and Wong et al. (2012). Fourth, the color of the ETG sequence is constant over the full density range (see red linear fit), while the color of the LTG sequence increases only very little by 0.1 mag in the low-mass regime (see blue linear fit). The apparent slope of the color as a function of density considering all galaxies (see black linear fit) is entirely due to a population effect: at high density the ETGs dominate in number. It is not clear if the color distribution is truly bimodal or, if we had not subdivided LTGs from ETGs by morphology, the red and the blue sequence would result in a single sequence that would progressively redden with increasing density.

3.4. Activity on nuclear scale

It is interesting to verify if the Hα morphology of HI-poor LTGs differs statistically from the HI-rich ones. To pursue this, we measured the total extended flux and the flux in the central 3 arcsec (mimicking the SDSS spectral fibers) of HI-poor LTGs
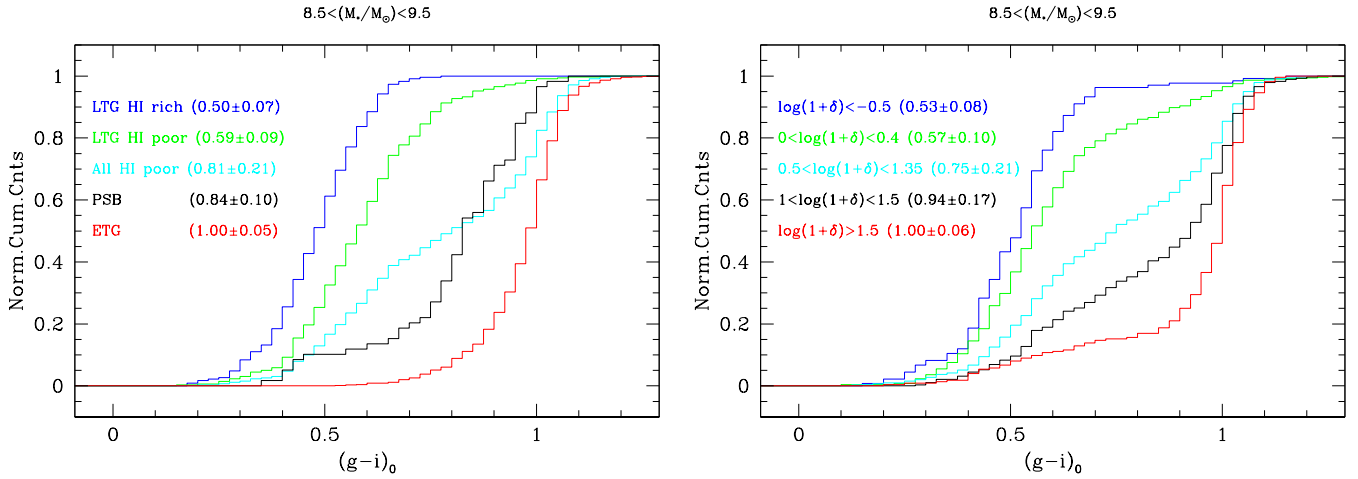
Fig. 8. Cumulative distributions of the $(g - i)_o$ color in the interval $8.5 < \log(M_*/M_\odot) < 9.5$, in the bins of morphological type/HI content (left panel) defined in Section 3.3 and in bins of local galaxy density (right panel). In parenthesis the median $(g - i)_o$ color with uncertainty is given. Notice the similarity between the distributions in the two panels.

in the Hα images. The cumulative distribution of the ratio of the two fluxes is given in Fig. 10 (green histogram). This distribution is significantly different from the one of HI-rich galaxies (blue histogram), because the Hα distribution of HI-poor galaxies is much more centrally concentrated. The HI-poor LTG galaxies appear to have some Hα emission that is for the most part confined to a central or even nuclear source[11]. A Kolmogorov-Smirnov test indicates that the probability that the two samples are drawn from the same parent population is $2 \times 10^{-9}\%$, i.e., they differ significantly. This is consistent with an Hα disk truncated by ram-pressure (Fumagalli & Gavazzi 2008), such as in the prototype NGC 4569 in Virgo (Boselli et al. 2006) or in NGC 4848 in Coma (Fossati et al. 2012). These cases are different from the HI-rich systems, which tend to host Hα emission extended across the entire disk (as discussed in Paper IV).

Figure 11 shows that HI-poor and HI-rich LTGs have an identical intensity of the nuclear Hα however. The figure shows the distribution of the Hα equivalent width (EW, a proxy for nuclear SSFR) as derived from the nuclear SDSS spectra versus the stellar mass separately for HI-rich (blue symbols) and HI-poor (green symbols) LTGs. Both subsamples show an identical mild decrease of the nuclear Hα EW with increasing mass (similar to the decrease of the diffuse SSFR with mass in Figure B.1 d), but apart from that they have an identical specific star formation activity in the nuclear region. A Kolmogorov-Smirnov test indicates that the probability that the two samples are drawn from the same parent population is 4.1 %, i.e., they do not differ by more than 2 sigma.

In conclusion, HI normal, low-mass LTGs have extended star-forming disks. The star formation shrinks to the nucleus when LTGs are affected by gas ablation, but on this scale the star formation occurs with the same intensity as in gas rich systems. Only ETGs become completely passive even in their nuclei (at stellar masses as low as $10^{9.5}$ $M_\odot$ AGNs of high and low activity (LINER) are practically absent even among ETGs, see Gavazzi et al. 2011). This provides solid evidence that the mechanism that produces the quenching of the star formation

Fig. 9. Blue and red sequence traced by the $(g-i)_o$ color as a function of the local galaxy density in two bins of stellar mass, below (bottom) and above (top) $\log(M_*) = 9.5$. Blue symbols mark LTGs, while ETGs are given with red symbols. The two populations are fitted separately (colored lines) and together (black line). The black points represent PSBs.

proceeds outside-in, as in the ram-pressure scenario. Other processes such as tidal interactions would truncate the star formation in the outer disks, but would increase it as well on the nuclear scale (Kennicutt et al. 1987, see however Bretherton et al. 2010, who claimed some role of tidal mechanisms in cluster galaxies). In contrast, milder ablation processes such as starvation could produce a cut-off of the cold gas supply and in turn a significant quenching of the star formation even in galaxy groups (as supported by numerical simulations by Kawata & Mulchaey 2008). However, this mechanism is not expected to reproduce the truncated HI disks (Cayatte et al. 1994, Chung et al. 2009) and the truncated Hα profiles (Koopmann & Kenney 1998, 2004; Boselli et al. 2006) observed in cluster galaxies.

---

[11] In order to protect against size effects, we have recomputed the flux ratio in Fig. 10 using a variable inner aperture of 3, 6 and 9 arcsec, each chosen according to the overall size of the galaxies. Our conclusions remain unchanged.
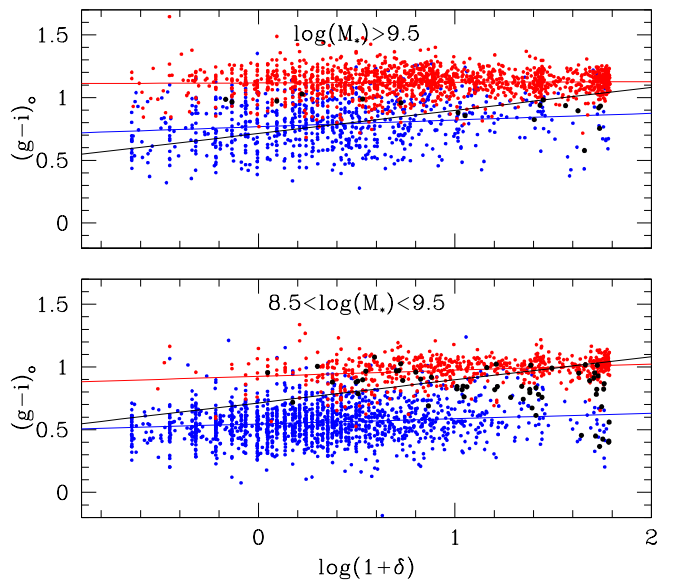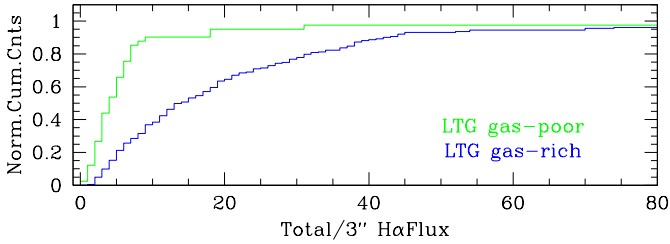
Fig. 10. Cumulative distribution of the ratio of total Hα flux to Hα flux measured in a central 3-arcsec aperture in the imaging material. The blue histogram refers to LTGs detected in ALFALFA (HI-rich) and the green one depicts LTGs not detected in ALFALFA (HI-poor).
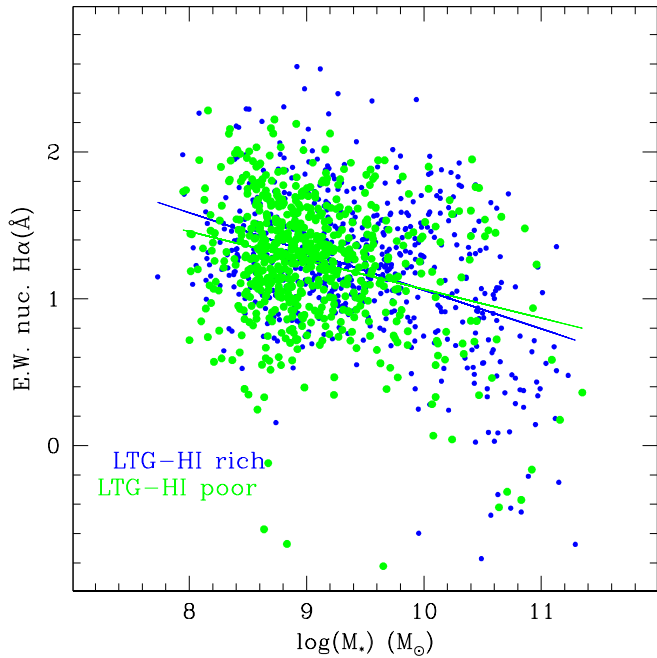

Fig. 11. E.W. of the Hα line as derived from nuclear SDSS spectra versus stellar Mass of LTG galaxies (in subsamples 2). Galaxies are color-coded as follows: green=LTG-not in ALFALFA (HI-poor); blue=LTG-in ALFALFA (HI-rich).

3.5. Local density or velocity dispersion?

It is also interesting to check if the transformation just found, i.e., the progressive reduction of the star formation with increasing density, occurs only in the environment of rich galaxy clusters or also in galaxy groups. For this we studied a possible dependence of the fraction of HI-rich LTGs on the velocity dispersion σ of the groups/cluster that host them. This is because σ traces the potential well of the hosting galaxy systems and, as a consequence, is directly and physically linked to the strength of the ram-pressure process (Gunn & Gott 1972, Domainko et al. 2006). We developed a two-step automatic procedure that identifies and characterizes the galaxy groups in region 2. The first step identifies galaxies that can be considered tracers of galactic groups. A tracer must lie in an overdensity with at least 20 members within a circle of 0.3 degree (530 kpc) radius. σ and the

mean recessional velocity $\langle Vel \rangle$ were estimated for each tracer by averaging over its neighbors up to a maximum number of 30 galaxies. This allows for a more detailed description of the "local" sigma value in the highest density regions like, e.g., the Coma cluster. Once the tracers were identified, the code proceeded with step II, in which the membership of each individual LTG to a group/cluster was checked. To be hosted by a group, a galaxy (*i*) must lie within a projected separation of 0.5 deg (900 kpc) and (*ii*) its velocity along the line of sight must not differ by more than 3 σ from $\langle Vel \rangle$. The code defines as "field" galaxy every object located more than 3 deg (5.3 Mpc) away from each overdensity. This conservative constraint slightly reduces the number statistics, but prevents any contamination from galaxies in the outskirts of the overdensities themselves.

The procedures identified seven groups and the Coma cluster, as listed in Table 1. The test discussed in Dressler & Shectman (1988) confirmed the substructures we found. This is to be expected because of the velocity criterion that we enforced to define the group elements. This criterion selects dynamically well-defined groups with a velocity dispersion quite a bit lower than the Coma cluster itself, as shown in Figure 12. For each group we computed the fraction of HI-rich LTGs with

Table 1. Properties of the seven groups found in region 2.

Group	Name	RA	Dec	N	$< V >$	σ
gr1	NGC 3651	170.7608	24.210	35	7745	455
gr2	NGC 4104	181.6839	28.172	27	8316	672
gr3	UGC 7115	182.0195	25.260	54	6627	427
gr4	NGC 4213	183.8709	23.916	12	6884	287
gr5	NGC 4555	188.8925	26.573	43	6615	309
gr6	UGC 8763	207.7632	25.039	37	8779	230
gr7	IC 4345	208.8824	25.126	23	8994	260

the associated Poissonian uncertainty. The fraction of HI-rich LTGs for the entire late-type population is plotted in Figure 12a as a function of the velocity dispersion and in Figure 12b as a function of the local galaxy density in three different environments: the large dot corresponds to the average fraction in the lowest density environment (field), the square is the fraction in the highest density environment (the Coma cluster) and the small dots correspond to seven individual groups, with the triangle showing their average value. Apparently, the fraction of HI-rich LTGs decreases with increasing local density (Figure 12b) (approximately 1 σ from isolated to groups and more than 4 σ from groups to clusters). However, considering the large statistical uncertainty on the gas-rich fraction, groups are truly intermediate between isolated and Coma galaxies, i.e., there is not definitive evidence that the entire decrease occurs in the densest environment.

Conversely, when the fraction HI-rich LTGs is plotted as a function of σ (Figure 12a), it becomes more clear that their fraction drops at $\sigma >> 100$ km s^{-1}, at the typical dispersion of Coma-like clusters (we caution, however, that the analysis presented in Figure 12 should be extended to comprise more Coma-like clusters before any strong conclusion can be drawn). Recent simulations by Bahe et al. (2012) have shown that the pressure exerted on the cold gas by the IGM is at least one order of magnitude higher in clusters than in groups. In addition, the efficiency of cold gas stripping is relevant only within the virial radius even for a massive cluster like Coma (see however Merluzzi et al. 2013), which renders a strong ram-pressure efficiency in groups

unlikely because it would require the infalling galaxy to pass very near the group center.

4. Discussion and conclusion

The environmental conditions occurring in the vicinity of an evolved cluster of galaxies such as the Coma cluster have well-known (Giovanelli & Haynes 1985) catastrophic consequences on the HI content of their member galaxies. However, HI observations deeper than ALFALFA are required to detect the pattern of HI deficiency (see Sections 3.1 and 3.2). At the distance of Coma ALFALFA is just sensitive enough ($\log(M_{HI}/M_\odot) \geq 9$) to separate optically selected LTGs into HI-poor and HI-rich galaxies.

The SSFR (see Figure 7c) of galaxies scales down with the galaxy stellar mass, but for the dwarf regime ($8.5 < \log(M_*/M_\odot) < 9.5$) there is a clear tendency for the median $(g - i)_o$ color to increase systematically (see Figure 8a) along the "morphological" sequence constituted by
1) HI-rich LTGs, the bluest objects with median $(g - i_o)$=0.50 mag;
2) HI-poor LTGs, with median $(g - i_o)$=0.60 mag;
3) PSBs, with median $(g - i_o)$=0.84 mag;
4) ETGs, with median $(g - i_o)$=1.00 mag.
The specific star formation rate decreases accordingly. Along this sequence there is a parallel sequence that refers to their nuclear properties: HI-rich LTGs have identical nuclear star formation activity as HI-poor LTGs (Figure 11), but their star formation extends over the whole disks, while HI-poor LTGs harbor some star formation exclusively on a circumnuclear scale (Figure 10). The star formation becomes entirely suppressed, even on nuclear scale in PSBs and ETGs. Whatever mechanism quenches the star formation, it proceeds outside-in, as in the ram-pressure scenario (see also Boselli et al. 2006, 2009).

A similar $(g - i)_o$ - stellar mass sequence is obtained by dividing galaxies into bins of increasing local density (Figure 7b and 8b). It appears indisputable that the local density has a main impact on the gas content and SF of galaxies, contributing to their morphological migration, i.e., HI-rich LTGs represent about 60% of the entire LTG population at low and intermediate galaxy density (comprising the cosmic filaments up to the groups) and drop to zero in the core of the Coma cluster. Conversely, HI-poor LTGs (representing the other 40% of the LTGs in isolation) increase in frequency with increasing density, becoming the majority of all LTGs in the core of Coma. This agrees with the analysis of Fabello et al. (2012) based on a $\log(M_*/M_\odot) \geq 10.0$ sample.

It is very tempting to interpret all these features as the results of a fast environmentally driven process that superposes to the standard and long-term evolutionary track that acts on field and group galaxies. Galaxies infalling toward a cluster are evolved by a process that causes some gas ablation, proceeding outside-in in two steps: 1) first a significant quenching of the global star formation is produced in the disk, resulting in redder colors, but without affecting the circumnuclear star formation; 2) the quenching of SF activity proceeds to the nuclear scale (transforming star-forming nuclei into passive ones, passing through the PSB phase). On a similar time scale, dwarf galaxies are transformed from LTGs to ETGs. The time scale for gas depletion is short enough ($\sim$ 100-300 Myr) to quickly transform HI-rich LTGs into anemic LTGs, which end up as gas-free, passive dEs. This is precisely the mechanism invoked by Boselli et al. (2008) and by Gavazzi et al. (2010) to migrate dwarf star-forming systems into dEs in the neighborhood of rich

galaxy clusters (see also Cortese & Hughes 2009 and Cortese et al. 2011). Meanwhile the ram pressure mechanism, owing to its short time scale, is also capable of producing a k+a signature in their spectra, thus enhancing the number of galaxies presenting some PSB phase toward rich clusters (Gavazzi et al. 2010; Wong et al. 2012) and making the number of active nuclei (both star forming and AGNs of various forms) decrease near the center of rich clusters (Gavazzi et al. 2011).

The dependence of this quenching process on the galaxy density and in particular on the galaxy velocity dispersion (it acts selectively on galaxies hosted in galaxy clusters, see Figure 12), together with the evidence that it proceeds from outside-in, make the ram-pressure mechanism (Gunn & Gott 1972) our favorite interpretation over strangulation (Larson et al. 1980) This conclusion should be taken with the grain of salt because it is based on one cluster (Coma) and should be confirmed with similar analysis of more clusters. In support of our conclusion, Merluzzi et al. (2013) found evidence for ram-pressure stripping well beyond 1 Mpc from the center of Abell 3558. In contrast the numerical simulations of Kawata & Mulchaey (2008) support the starvation mechanism as capable of cutting off the gas supply, hence of quenching the star formation even in galaxy groups.

We finally note that this fast evolutionary scenario could be used to constrain the build-up of the Coma cluster with cosmic time at the expenses of infalling galaxies, following the argument of Adami et al. (2005) for Coma and of Boselli et al. (2008) for Virgo. Assuming naively that the infall rate was constant over the past few Gyrs, this quantity can be estimated from the number of galaxies in each specific morphological stage divided by the typical time scale of each stage (to be precise, since this estimate is very sensitive to the sample completeness, the argument provides lower limits to the infall rate). Restricting this to galaxies with $\log(M_*/M_\odot) > 9$, to be consistent with a similar calculation carried out in Paper II for Virgo, we classified 26 HI-rich LTGs within the cluster. Assuming a characteristic time scale for the complete stripping of gas due to ram pressure of 300 Myr for massive galaxies such as NGC 4569 (Boselli et al. 2008)[12], we obtain a flux of infalling LTGs of $F_{gal} = 86 \, \text{Gyr}^{-1}$. We can cross-check this result with the independent constraint derived from the number of galaxies in the HI-poor phase (70) (that still show some circumnuclear star formation probably sustained by residual nuclear HI and H_2 anchored to the deep central potential well), divided by the time-scale of H_2 ablation. Assuming that a complete HI and H_2 removal will occur due to ram pressure during the second passage through the cluster center on a time-scale of 0.7 ± 0.4 Gyr (see Paper II), the infall rate is $F_{gal} = 100 \, \text{Gyr}^{-1}$. In passing we note that the time scale estimate we used is considerably shorter than that for complete consumption of the H_2 due to star formation of $\sim 2 \pm 1$ Gyr (Bigiel et al. 2008).

A similar argument holds for the 32 PSB galaxies observed in Coma. The PSB phase is expected to last up to 1.5 Gyr (Poggianti et al. 2009), but around 500 Myr in a blue continuum regime (see Fig. 20 in Boselli et al. 2008), such as in the 32 PSB galaxies analyzed here. Again, the galaxy flux toward Coma would be $F_{gal} = 64 \, \text{Gyr}^{-1}$, consistent with the previous estimates. Assuming that the age of the Coma cluster is about 7.5 Gyr (its formation took place approximately at z=1, Wechsler et al 2002), and that it is composed of about 750 galaxies, the infall rate would become $F_{gal} = 130 \, \text{Gyr}^{-1}$. All "order of magnitude"

---

[12] This estimate is reduced to 100 Myr for dwarf objects such as VCC 1217 (Fumagalli et al. 2011) or VCC 1249 in the M49 group (Arrigoni Battaia et al. 2012).
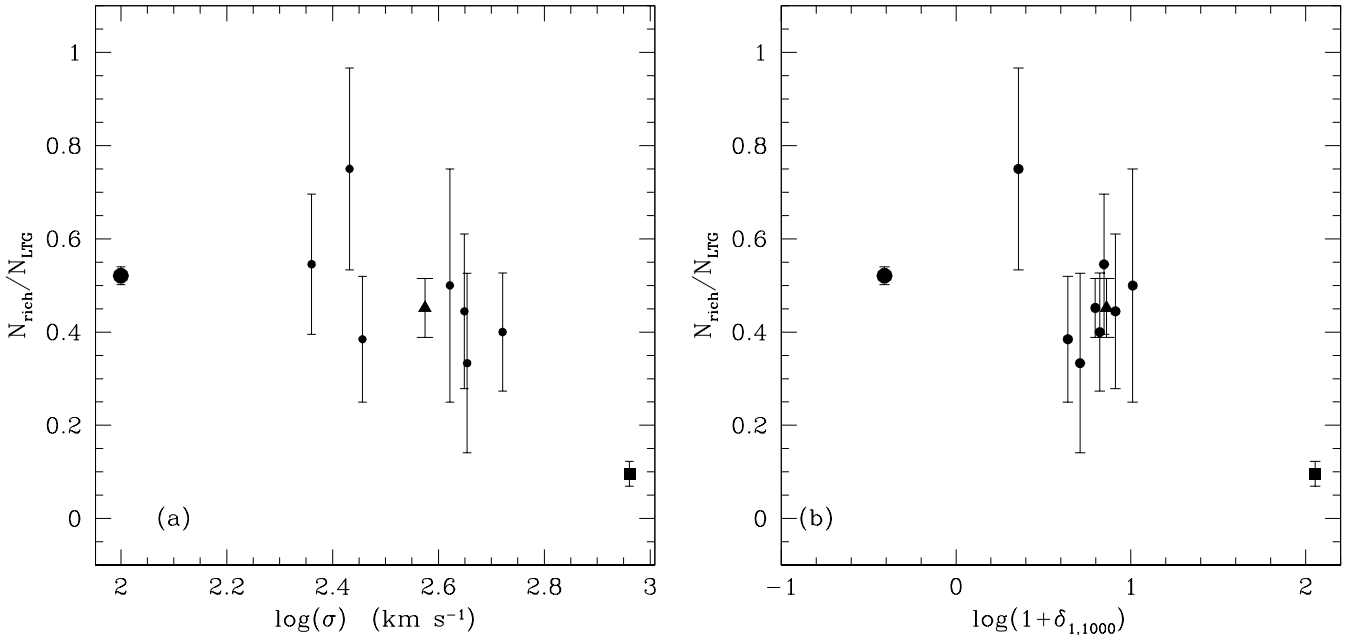
Fig. 12. The number ratio of HI-rich LTGs over all LTGs as a function of the velocity dispersion (panel a) and of the local density (panel b) of 7 groups (small dots) and their average (triangle), the Coma cluster (square) and the field (large dot). The last point has been plotted at 100 σ = km s^{-1} to represent that, even in the field, galaxies are subject to random motions.

estimates are consistent with one another within 30 percent from $F_{\mathrm{gal}} = 100$ Gyr^{-1}, i.e., a constant galaxy flow building the cluster over a large portion of the cosmic time, as was concluded by Adami et al. (2005). Consistent infall rate, sustained for 2 Gyr, has been claimed to feed the younger Virgo cluster (Paper II).

The infall rate estimate can be checked for consistency with semi-analytic models of halo formation, e.g., Wechsler et al (2002). From their Figure 3 we derive that cluster-like halos accreted 70% of their final mass in the last 7.5 Gyr (the assumed age of the Coma cluster). If one takes for Coma a current halo mass of approximately 10^{14} M$_\odot$, the average growth is 10^{13} M$_\odot$ Gyr^{-1}. Considering (very crudely) that this accretion is contributed by galaxy halos of 10^{11} M$_\odot$ each, the derived accretion rate is 100 galaxies per Gyr on average, in agreement with our previous estimate.

Table 2. Build-up of the Coma cluster from various estimators.

	All	PSB	HI-poor	HI-rich
N (log(M_*/M$_\odot$) > 9)	750	32	70	26
t (Gyr)	7.5 ± 1	0.5 ± 0.2	0.7 ± 0.4	0.3 ± 0.1
Infall rate (Gyr^{-1})	100 ± 14	64 ± 28	100 ± 58	86 ± 33

Appendix A: empirical correction for internal extinction

An exhaustive treatment of the internal extinction correction to the u, g, r, i, z magnitudes is beyond the scope of this work and will be addressed in a forthcoming paper. We concentrate on a less ambitious task, i.e., on the empirical method for correcting the color magnitude relation for the effects of internal extinction. The color ($g - i$) versus stellar mass diagram (see Figure A.1, color-coded according to the Hubble type) composed of all optically selected galaxies (regions 1 and 2) contains a well-developed red-sequence (e.g. Hogg et al. 2004) mostly composed of ETGs along with the so-called blue cloud, mostly composed of LTGs. When magnitudes are not corrected for internal extinction the two color sequences, that are well separated at low mass by the green valley, overlap one another at the high-mass end. This is an obvious consequence of the increasing internal extinction suffered by disk galaxies of increasing mass. Given the abundant number statistics offered by SDSS, it is possible to investigate this effect as a function of galaxy inclination in the plane of the sky. For disk galaxies (Sa through Sdm) the inclination *incl* with respect to the line of sight was computed following Solanes et al. (1996) assuming that spirals are oblate spheroids of intrinsic axial ratio q:

$$\cos^2(incl) = \frac{(b/a)^2 - q^2}{1 - q^2}, \tag{A.1}$$

where a and b are the major and minor axes. Intrinsic axial ratios were assumed to be equal to the modal values of the distribution of true ellipticities of galaxies of different Hubble types in the Second Reference Catalog of Bright Galaxies (de Vaucouleurs, de Vaucouleurs, & Corwin 1976). For the giant spirals these are $q = 0.32$ for Sa, $q = 0.23$ for Sab, and $q = 0.18$ for Sb-Sc. Whenever $b/a < q$, *incl* is set to 90°. Irregulars+BCD (mostly low-mass objects) do not have this parameter defined, because their axial ratio does not give a measure of the inclination of the disk, but of their intrinsic triaxiality.

Figure A.2 (top panel) shows the $g - i$ color versus stellar mass diagram for LTGs in regions 1+2 considering only nearly edge-on (*incl* > 80) and nearly face-on (*incl* < 30) galaxies, with the best linear fit. It is evident that the fits cross each other near

$\log M_* = 8.0$, i.e., the extinction correction is null near $\log M_* = 8.0$, and it increases with increasing stellar mass as a function of the inclination. The slope of the relation as a function of the cosine of the inclination is given in Figure A.2 (bottom panel). This relation can be used to extrapolate $g-i$ to the face-on value, or to obtain the color correction for internal extinction:

$$(g-i)_o = (g-i) - \left\{ +0.17 \cdot [1-\cos(incl)] \cdot \left[\log\left(\frac{M_*}{M_\odot}\right) - 8.19 \right] \right\}, \text{(A.2)}$$

where *incl* is the galaxy inclination. After applying the empirical internal extinction correction the resulting slope of the LTG sequence becomes similar to the one of ETGs, and the green-valley opens up over the full interval of masses (Figure A.1 - bottom panel). Note the difference between the correction method proposed here (which depends on a combination of M_* and *incl*) and the one proposed by Yip et al. (2011), which purely depends on *incl*.

Appendix B: Scaling relations

Hα3, which is based on an ALFALFA-selected sample in the Coma supercluster provides us with insufficient coverage of HI mass, stellar mass, and SFR because of the shallowness of ALFALFA at the distance of Coma. Therefore the analysis of the scaling relation among the HI gas content and the stellar mass of galaxies cannot be undertaken with a sufficient dynamical range of HI mass, stellar mass, and SFR. However by adding the results of the present survey with similar ones obtained in Paper II for the Local Supercluster (where the ALFALFA sensitivity is 35 times better), we broaden the dynamic range to four decades in stellar mass, obtaining the relations shown in Figure B.1, whose linear regression parameters are listed in Table B.1. The data obtained in this paper for the Coma supercluster for galaxies with $Def_{HI} \le 0.2$ are plotted separately (blue symbols) from those in the Local Supercluster with $Def_{HI} \le 0.3$ taken from paper II (light gray). AGNs of various levels of activity are identified in Figure B.1 (with asterisks) according to the criteria of Gavazzi et al. (2011).

We begin by studying the relation between M_{HI} and M_*, as shown in Figure B.1 (a). The diagonal lines represent the sensitivity limit of ALFALFA, computed for galaxies with an inclination of 45 deg (see Section 2.2). The dotted line is computed for the distance of the Virgo cluster (17 Mpc), while the dashed one is for the distance of Coma (100 Mpc). Clearly the observed distribution for Coma lies very close to the line of limiting sensitivity, making the observed slope (0.34) spuriously shallow because galaxies near $\log(M_*/M_\odot) \sim 8$ and $\log(M_{HI}/M_\odot) \sim 8$, which are present locally, would not be detected at the distance of Coma. However, at the high-mass end of the stellar mass function, where the sampling is more abundant in Coma than locally because of the larger volume, no selection effects would prevent us from detecting galaxies if they had the same steep slope as extrapolated from the Local Supercluster. Therefore we conclude that the change of slope seen in Figure B.1 (a) near $\log(M_*/M_\odot) \sim 9$ is real. A relation similar to the one in Figure B.1(a) and (b), i.e., significant flattening above $\log(M_*/M_\odot) \sim 8$, has been obtained by Huang et al. (2012) using the whole α.40 sample. They interpreted the flattening as a possible evidence of increasing gas loss due to AGN feedback with increasing mass.

We note that the observed relation, both in the steep part (0.47) and in the shallow (0.32), is nonetheless significantly shallower than the direct proportionality, as already discussed in Gavazzi et al. (2008) and in Paper II, reflecting a genuine non-proportionality between the two quantities. When the HI
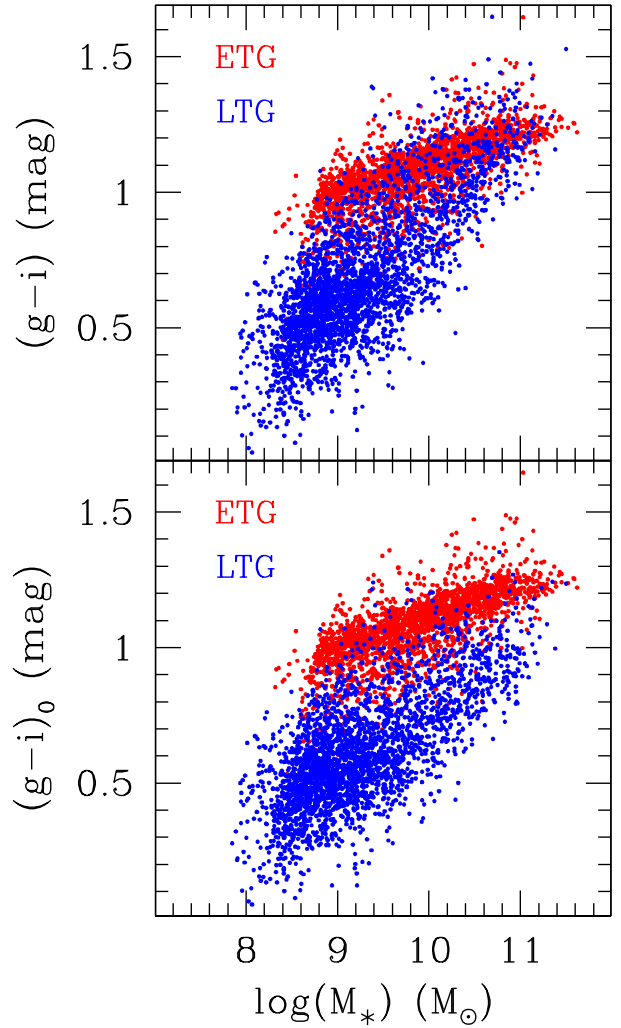

Fig. A.1. (top): observed color $(g - i)$ -stellar mass diagram of all 5026 optically selected galaxies from SDSS (subsamples 1+2) divided by morphological types: ETGs (dE-S0a, red), LTG (Sa-Im-BCD, blue). Many high-mass LTGs overlap with, or are even redder than, ETGs of similar mass. (bottom): same as above but $(g - i)_o$ is corrected for inclination as described in this appendix. The correction is visible at high mass where LTGs have now bluer colors than ETGs. The blue and red sequence become more parallel and a significant green valley opens up between them.

gas fraction M_{HI}/M_* is plotted as a function of the stellar mass (Figure B.1 b), the fraction of gas decreases by approximately 2 orders of magnitude with increasing galaxy mass, from $\log(M_*/M_\odot) \sim 7.5$ to ~ 11.5. In other words, $10^{7.5}$ $M_\odot$ galaxies contain ten times more gas than stars. This ratio is reduced to less than 10% in $10^{11.5}$ $M_\odot$ systems. This basic result agrees perfectly with what was found in the (optically selected) GASS survey by Catinella et al. (2010) in the stellar mass range $10^{10} < M_* < 10^{11.5}$ $M_\odot$ and by Cortese et al. (2011) for HI-normal galaxies in the Herschel Reference Survey (HRS; Boselli et al. 2010). It is also consistent with the *downsizing* scenario (Gavazzi 1993, Gavazzi et al. 1996, Cowie et al. 1996; Gavazzi & Scodeggio 1996, Boselli et al. 2001, Fontanot et al. 2009), where progressively more massive galaxies have less gas-to-star ratio at $z=0$ because they have transformed most of their gas into stars at higher z, while dwarf LTGs retain large quantities of hy-
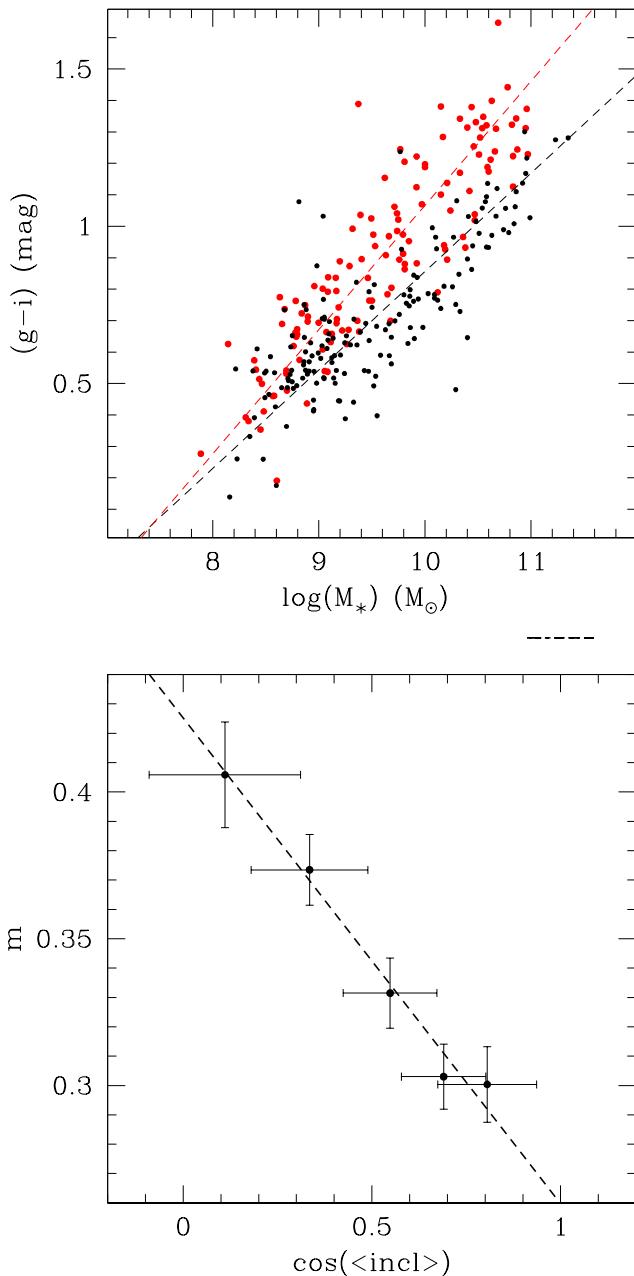
Fig. A.2. (Top panel) Observed color $(g-i)$ -stellar mass diagram (sub-samples 1+2) of edge-on LTGs ($incl > 80$, red) and of face-on LTGs ($incl < 30$, black), each with the linear best fit (dashed line). (Bottom panel) The slope of the fit to the color $(g-i)$ -stellar Mass relation of disk galaxies (Sa-Sdm) (see Figure A.2) as a function of galaxy inclination.

drogen capable of sustaining the star formation at some significant rate at the present cosmological epoch.

Similarly, we find that the relation between the SFR and the stellar mass (Figure B.1 c) and that of the specific SFR with stellar mass (d) are consistent with a change of slope around $\log(M_*/M_\odot) \sim 9$. Below that threshold a steeper dependence (0.8, i.e., almost of direct proportionality) is traced by the local galaxies. Above this limit the relation is much shallower (0.33) and is followed by the more distant Coma galaxies. Consequently, in the range of stellar mass covered by the Coma supercluster the specific star formation rate decreases sig-

nificantly with increasing mass, as found by Boselli et al. (2001), Bothwell et al. (2009) and by Schiminovich et al. (2010). This is again consistent with the "downsizing" scenario. At lower mass the relation flattens out and the scatter increases by 2 orders of magnitude, as noted by other authors (Lee at al. 2007, Bothwell et al. 2009). The curvature in Figure B.1 resulting from the superposition of the local and Coma superclusters is consistent with the change of slope found by Huang et al. (2012) in $\alpha.40$.

Table B.1. Linear regression coefficients of the relations in Figures B.1(a) through (d) (only for $Def_{HI} < 0.2$) obtained using the bisector method (mean coefficients of the direct and the inverse relation). C=Coma, V=Virgo (Paper II)

Linear regression	r	sample	Fig.B.1
$\log M_{HI} = 0.34\times \log M_* + 6.25$	0.76	C	a
$\log M_{HI} = 0.47\times \log M_* + 4.71$	0.85	V	a
$\log M_{HI} = 0.52\times \log M_* + 4.54$	0.84	V+C	a
$\log M_{HI}/M_* = -0.68\times \log M_* + 6.50$	-0.92	C	b
$\log M_{HI}/M_* = -0.69\times \log M_* + 6.12$	-0.90	V	b
$\log M_{HI}/M_* = -0.71\times \log M_* + 6.58$	-0.86	V+C	b
$\log SFR = 0.33\times \log M_* - 3.71$	0.52	C	c
$\log SFR = 0.80\times \log M_* - 8.04$	0.88	V	c
$\log SFR = 0.64\times \log M_* - 6.75$	0.85	V+C	c
$\log SSFR = -0.70\times \log M_* - 3.43$	-0.79	C	d
$\log SSFR = -0.26\times \log M_* - 7.53$	-0.53	V	d
$\log SSFR = -0.41\times \log M_* - 6.23$	-0.72	V+C	d

References

Abazajian, K. N., et al. 2009, ApJS, 182, 543
Adami, C., Biviano, A., Durret, F., & Mazure, A. 2005, A&A, 443, 17
Arrigoni Battaia, F., Gavazzi, G., Fumagalli, M., et al. 2012, A&A, 543, A112
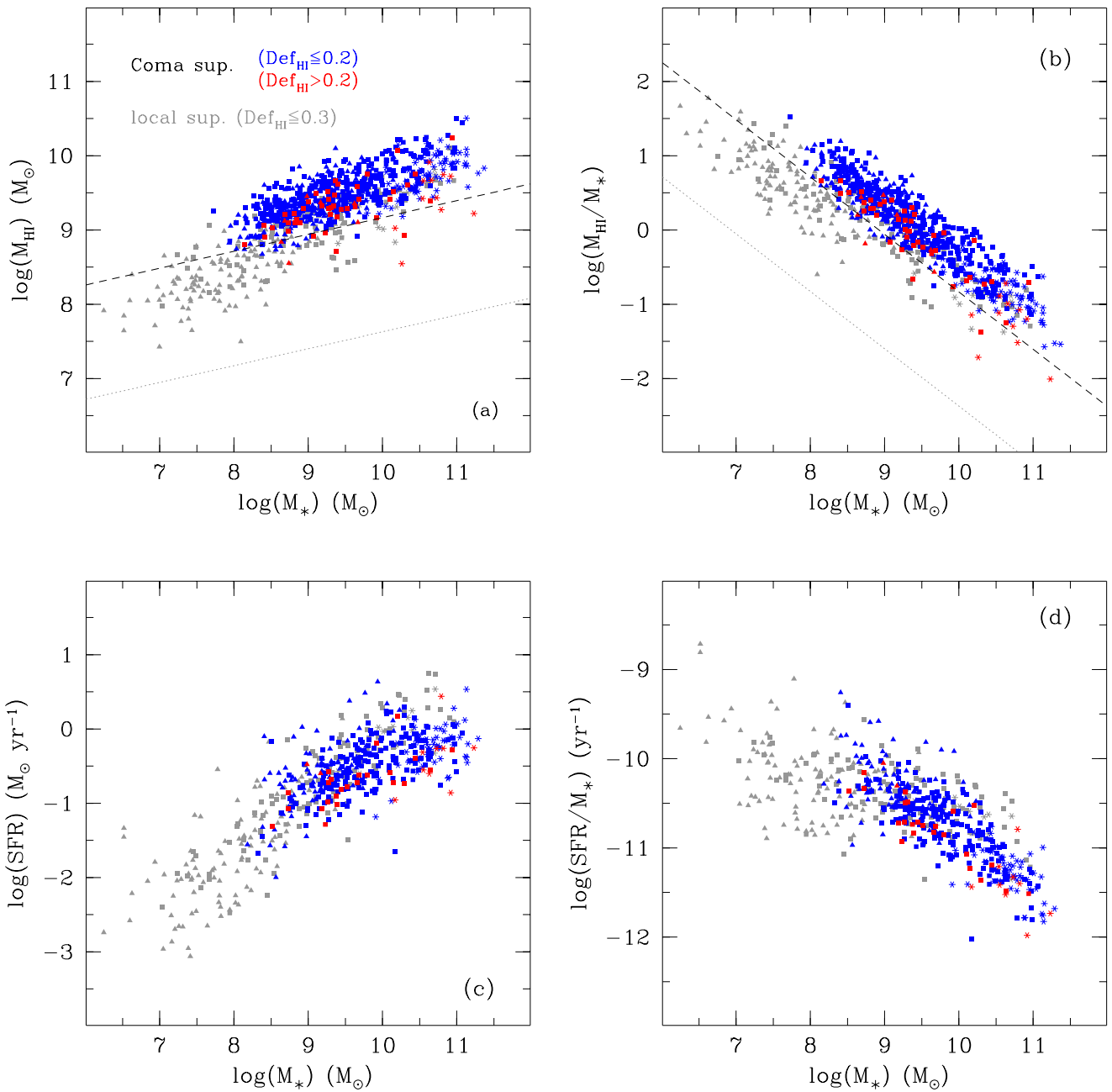Bahe Y. et al. 2012, arXiv:1210.8407

Fig. B.1. Principal scaling relations between M_{HI}, M_*, and SFR in the Coma supercluster covered by ALFALFA. Blue: $Def_{HI} \leq 0.2$; red: $Def_{HI} \geq 0.2$ compared to the $Def_{HI} \leq 0.3$ in the Local Supercluster (grey, Paper II). Symbols are assigned according to the morphology: spirals (Sa-Sdm): squares; Irr-BCD: triangles; AGN: asterisks. Top-left panel: the M_{HI} versus M_* relation The diagonal lines represent the limiting sensitivity of ALFALFA (computed for a mean $incl = 45^o$) at the distance of Virgo (gray dotted) and of Coma (black dashed). The shallow sensitivity of ALFALFA limits significantly the detection of galaxies at the distance of Coma, in particular with decreasing stellar mass. Top-right panel: the HI gas fraction (M_{HI}/M_*) versus M_*. Bottom-left panel: the relation between the SFR and the stellar mass. Bottom-right panel: the specific star formation rate versus stellar mass.

Bell, E. F., McIntosh, D. H., Katz, N., & Weinberg, M. D. 2003, ApJS, 149, 289

Bigiel, F., Leroy, A., Walter, F., Brinks, E., de Blok, W. J. G., Madore, B., & Thornley, M. D. 2008, AJ, 136, 2846

Blanton, M. R., Schlegel, D. J., Strauss, M. A., et al. 2005, AJ, 129, 2562

Boselli, A., Gavazzi, G., Donas, J., & Scodeggio, M. 2001, AJ, 121, 753

Boselli, A., & Gavazzi, G. 2002, A&A, 386, 124

Boselli, A., Iglesias-Páramo, J., Vílchez, J. M., & Gavazzi, G. 2002b, A&A, 386, 134

Boselli, A. & Gavazzi, G. 2006, PASP, 118, 517

Boselli, A., & Gavazzi, G. 2009, A&A, 508, 201

Boselli, A., Boissier, S., Cortese, L., et al. 2006, ApJ, 651, 811

Boselli, A., Boissier, S., Cortese, L., & Gavazzi, G. 2008, ApJ, 674, 742

Boselli, A., Boissier, S., Cortese, L., Buat, V., Hughes, T. M., & Gavazzi, G. 2009, ApJ, 706, 1527

Boselli, A., Hughes, T. M., Cortese, L., Gavazzi, G., & Buat, V. 2013, A&A, 550, A114

Bothwell, M. S., Kennicutt, R. C., & Lee, J. C. 2009, MNRAS, 400, 154

Bretherton, C. F., James, P. A., Moss, C., & Whittle, M. 2010, A&A, 524, A24

Catinella, B., Schiminovich, D., Kauffmann, G., et al. 2010, MNRAS, 403, 683

Cayatte, V., Kotanyi, C., Balkowski, C., & van Gorkom, J. H. 1994, AJ, 107, 1003

Chung, A., van Gorkom, J. H., Kenney, J. D. P., Crowl, H., & Vollmer, B. 2009, AJ, 138, 1741

Cortese, L., & Hughes, T. M. 2009, MNRAS, 400, 1225

Cortese, L., Catinella, B., Boissier, S., Boselli, A., & Heinis, S. 2011, MNRAS, 415, 1797

Cowie, L. L., Songaila, A., Hu, E. M., & Cohen, J. G. 1996, AJ, 112, 839

Domainko, W., Mair, M., Kapferer, W., et al. 2006, A&A, 452, 795

Dressler, A., & Shectman, S. A. 1988, AJ, 95, 985

Fabello, S., Kauffmann, G., Catinella, B., et al. 2012, MNRAS, 427, 2841

Fontanot, F., De Lucia, G., Monaco, P., Somerville, R. S., & Santini, P. 2009, MNRAS, 397, 1776

Fossati, M., Gavazzi, G., Boselli, A., & Fumagalli, M. 2012, A&A, 544, A128

Fossati, M., Gavazzi, G., Savorgnan, G., Fumagalli M., Boselli, A., Gutierrez, L., H. Hernandez Toledo, Giovanelli, R., Haynes, M. P., Paper IV, 2013, A&A, Submitted

Fumagalli, M., & Gavazzi, G. 2008, A&A, 490, 571

Fumagalli, M., Gavazzi, G., Scaramella, R., et al. 2011b, A&A, 528, 46

Gavazzi, G. 1993, ApJ, 419, 469

Gavazzi, G., Pierini, D., & Boselli, A. 1996, A&A, 312, 397

Gavazzi, G., & Scodeggio, M. 1996, A&A, 312, L29

Gavazzi, G., Boselli, A., Scodeggio, M., Pierini, D., & Belsole, E. 1999, MNRAS, 304, 595

Gavazzi, G., Boselli, A., Pedotti, P., Gallazzi, A., & Carrasco, L. 2002a, A&A, 386, 114

Gavazzi, G., Boselli, A., Pedotti, P., Gallazzi, A., & Carrasco, L. 2002b, A&A, 396, 449

Gavazzi, G., Boselli, A., Donati, A., Franzetti, P., & Scodeggio, M. 2003, A&A, 400, 451

Gavazzi, G., Zaccardo, A., Sanvito, G., Boselli, A., & Bonfanti, C. 2004, A&A, 417, 499

Gavazzi, G., Boselli, A., van Driel, W., & O'Neil, K. 2005, A&A, 429, 439

Gavazzi, G., Boselli, A., Cortese, L., et al. 2006, A&A, 446, 839

Gavazzi, G., Giovanelli, R., Haynes, M. P., et al. 2008, A&A, 482, 43

Gavazzi, G., Fumagalli, M., Cucciati, O., & Boselli, A. 2010, A&A, 517, A73

Gavazzi, G., Savorgnan, G., & Fumagalli, M. 2011, A&A, 534, A31

Gavazzi, G., Fumagalli, M., Galardo, V., Grossetti, F., Boselli, A., Giovanelli, R., Haynes, M. P. & Fabello, S., Paper I, 2012, A&A, 545, A16

Gavazzi, G., Fumagalli, M., Galardo, V., Grossetti, F., Boselli, A., Giovanelli, R.& Haynes, M. P., Paper II, 2013, submitted to A&A

Giovanelli, R., & Haynes, M. P. 1985, ApJ, 292, 404

Giovanelli, R., Haynes, M. P., Kent, B. R., et al. 2005, AJ, 130, 2598

Giovanelli, R., Haynes, M. P., Kent, B. R., et al. 2007, AJ, 133, 2569

Gunn, J. E., & Gott, J. R., III 1972, ApJ, 176, 1

Haynes, M. P., & Giovanelli, R. 1984, AJ, 89, 758

Haynes, M. P., & Giovanelli, R. 1986, ApJ, 306, 466

Haynes, M. P., Giovanelli, R., Martin, A. M., et al. 2011, AJ, 142, 170

Hogg, D. W., Blanton, M. R., Brinchmann, J., et al. 2004, ApJ, 601, L29

Huang, S., Haynes, M. P., Giovanelli, R., & Brinchmann, J. 2012, ApJ, 756, 113

Iglesias-Páramo, J., Boselli, A., Cortese, L., Vílchez, J. M., & Gavazzi, G. 2002, A&A, 384, 383

Isobe, T., Feigelson, E. D., Akritas, M. G., & Babu, G. J. 1990, ApJ, 364, 104

James, P. A., et al. 2004, A&A, 414, 23

Kawata, D., & Mulchaey, J. S. 2008, ApJ, 672, L103

Kennicutt, R. C., Jr., Roettiger, K. A., Keel, W. C., van der Hulst, J. M., & Hummel, E. 1987, AJ, 93, 1011

Kennicutt, R. C., Jr., Lee, J. C., Funes, S. J., José G., Sakai, S., & Akiyama, S. 2008, ApJS, 178, 247

Koopmann, R. A., & Kenney, J. D. P. 1998, ApJ, 497, L75

Koopmann, R. A., & Kenney, J. D. P. 2004, ApJ, 613, 866

Larson, R. B., Tinsley, B. M., & Caldwell, C. N. 1980, ApJ, 237, 692

Lee, J. C., Kennicutt, R. C., Funes, S. J., José G., Sakai, S., & Akiyama, S. 2007, ApJ, 671, L113

Lee, J. C., Gil de Paz, A., Tremonti, C., et al. 2009, ApJ, 706, 599

Martin, A. M., Papastergis, E., Giovanelli, R., et al. 2010, ApJ, 723, 1359

Mendel, J.T., et al. 2013, arXiv:1211.6115

Merluzzi, P., Busarello, G., Dopita, M. A., et al. 2013, MNRAS, 429, 1747

Meurer, G. R., Hanish, D. J., Ferguson, H. C., et al. 2006, ApJS, 165, 307

Poggianti, B. M., Aragón-Salamanca, A., Zaritsky, D., et al. 2009, ApJ, 693, 112

Saintonge, A. 2007, AJ, 133, 2087

Salim, S., Rich, R. M., Charlot, S., et al. 2007, ApJS, 173, 267

Schiminovich, D., Catinella, B., Kauffmann, G., et al. 2010, MNRAS, 408, 919

Solanes, J. M., Giovanelli, R., & Haynes, M. P. 1996, ApJ, 461, 609

Toribio, M. C., Solanes, J. M., Giovanelli, R., Haynes, M. P., & Masters, K. L. 2011, ApJ, 732, 92 .

Tremonti, C. A., Heckman, T. M., Kauffmann, G., et al. 2004, ApJ, 613, 898

Yip, C.-W., Szalay, A. S., Carliles, S., & Budavári, T. 2011, ApJ, 730, 54

Wechsler, R. H., Bullock, J. S., Primack, J. R., Kravtsov, A. V., & Dekel, A. 2002, ApJ, 568, 52

Wong, O. I., Schawinski, K., Kaviraj, S., et al. 2012, MNRAS, 420, 1684